Complex Organic Molecules in Star-Forming Regions of the Magellanic Clouds

Marta Sewiło,[*,†,‡] Steven B. Charnley,[¶] Peter Schilke,[§] Vianney Taquet,[‖] Joana M. Oliveira,[⊥] Takashi Shimonishi, Eva Wirström, Remy Indebetouw, Jacob L. Ward, Jacco Th. van Loon, Jennifer Wiseman, Sarolta Zahorecz, Toshikazu Onishi, Akiko Kawamura, C.-H. Rosie Chen, Yasuo Fukui, and Roya Hamedani Golshan

†*CRESST II and Exoplanets and Stellar Astrophysics Laboratory, NASA Goddard Space Flight Center, Greenbelt, MD 20771, USA*

‡*Department of Astronomy, University of Maryland, College Park, MD 20742, USA*

¶*Astrochemistry Laboratory, NASA Goddard Space Flight Center, Greenbelt, MD 20771, USA*

§*I. Physikalisches Institut der Universität zu Köln, Zülpicher Str. 77, 50937, Köln, Germany*

‖*INAF, Osservatorio Astrofisico di Arcetri, Largo E. Fermi 5, 50125 Firenze, Italy*

⊥*Lennard-Jones Laboratories, Keele University, ST5 5BG, UK*

E-mail: marta.m.sewilo@nasa.gov

Abstract

The Large and Small Magellanic Clouds (LMC and SMC), gas-rich dwarf companions of the Milky Way, are the nearest laboratories for detailed studies on the formation and survival of complex organic molecules (COMs) under metal poor conditions. To

date, only methanol, methyl formate, and dimethyl ether have been detected in these galaxies – all three toward two hot cores in the N113 star-forming region in the LMC, the only extragalactic sources exhibiting complex hot core chemistry. We describe a small and diverse sample of the LMC and SMC sources associated with COMs or hot core chemistry, and compare the observations to theoretical model predictions. Theoretical models accounting for the physical conditions and metallicity of hot molecular cores in the Magellanic Clouds have been able to broadly account for the existing observations, but fail to reproduce the dimethyl ether abundance by more than an order of magnitude. We discuss future prospects for research in the field of complex chemistry in the low-metallicity environment. The detection of COMs in the Magellanic Clouds has important implications for astrobiology. The metallicity of the Magellanic Clouds is similar to galaxies in the earlier epochs of the Universe, thus the presence of COMs in the LMC and SMC indicates that a similar prebiotic chemistry leading to the emergence of life, as it happened on Earth, is possible in low-metallicity systems in the earlier Universe.

Keywords

Magellanic Clouds, star formation, astrochemistry, complex organic molecules, molecular abundances

1 Introduction

An important issue for astrochemistry is to understand how the organic chemistry in low-metallicity environments (i.e., with low abundances of elements heavier than hydrogen or helium), relevant for star formation at earlier epochs of cosmic evolution, differs from that in the Galaxy. Large aromatic organic molecules such as polycyclic aromatic hydrocarbons (PAHs) are detected in high-redshift galaxies, but the formation efficiency of smaller complex organic molecules has been unknown. A quantitative determination of the organic chemistry

in high-redshift galaxies with different star formation histories, and lower abundances of the important biogenic elements (C, O, N, S, P), can shed light on the inventory of complex organic molecules available to planetary systems and their potential for harboring life (e.g.[1]). The nearest laboratories for detailed studies of star formation under metal poor conditions are the Large and Small Magellanic Clouds (LMC and SMC).

The LMC and SMC are gas-rich dwarf companions of the Milky Way located at a distance of (50.0 ± 1.1) kpc[2] and (62.1 ± 2.0) kpc[3], respectively. They are the nearest star-forming galaxies with metallicities Z (the mass fractions of all the chemical elements other than hydrogen and helium) lower than that in the solar neighborhood ($Z_\odot = 0.0134$)[4]: $Z_{\rm LMC}$∼0.3–0.5 $Z_\odot$ and $Z_{\rm SMC}$∼0.2 $Z_\odot$.[5,6] Apart from the lower elemental abundances of gaseous C, O, and N atoms (e.g.,[7]), low metallicity leads to less shielding (due to the lower dust abundance; e.g.,[8,9]), greater penetration of UV photons into the interstellar medium, and consequently warmer dust grains (e.g.,[10,11]). The interstellar ultraviolet radiation field in the LMC and SMC is 10–100 higher than typical Galactic values (e.g.,[12]). Gamma-ray observations indicate that the cosmic-ray density in the LMC and SMC is, respectively, ∼25% and ∼15% of that measured in the solar neighborhood ([13,14]). All these low metallicity effects may have direct consequences on the formation efficiency and survival of COMs, although their relative importance remains unclear.

The range of metallicities observed in the Magellanic Clouds is similar to galaxies at redshift $z \sim 1.5-2$, i.e. at the peak of the star formation in the Universe (between ∼2.8 and ∼3.5 billion years after the Big Bang; e.g.,[15]), making them ideal templates for studying star formation and complex chemistry in low-metallicity systems in an earlier Universe where direct measurements of resolved stellar populations are not possible. Only very recently have gaseous complex organic molecules (methanol: CH_3OH, methyl formate: $HCOOCH_3$, dimethyl ether: CH_3OCH_3) been detected in the LMC[16–18] and in the SMC[19], using the Atacama Large Millimeter/submillimeter Array (ALMA). These observations showed that interstellar complex organic molecules (COMs) can form in the low-metallicity environ-

ments, probably in the hot molecular cores and corinos associated with massive and low- to intermediate-mass protostars, respectively. COMs had previously been detected outside the Milky Way, but in galaxies with metallicities comparable to or higher than solar ([20] and references therein).

In this article, we summarize the current state of knowledge concerning the organic chemistry in the Magellanic Clouds.

2 Molecular Line Inventories in Star-Forming Regions in the Magellanic Clouds

The proximity of the LMC/SMC enables both detailed studies of individual star-forming regions and statistical studies of molecular clouds or stellar populations on galactic scales. The systematic studies of molecular clouds in the Magellanic Clouds started with the ^{12}CO $J = 1 - 0$ survey of the LMC (central $6^\circ \times 6^\circ$;[22]) and the SMC ($2^\circ \times 2^\circ$,[23]) with a resolution of $8\farcm8$ (the Columbia 1.2m Millimeter-WaveTelescope), followed by a higher resolution ($2\farcm6$) survey of both galaxies with the NANTEN 4m telescope (e.g.,[24,25]). The more sensitive NANTEN survey that identified 272 molecular clouds in the LMC was published by.[26] The most luminous CO clouds from this survey were observed with $45''$ resolution using the Australia Telescope National Facility (ATNF) Mopra 22-m Telescope (the MAGMA survey;[27]).

The molecular gas in the Magellanic Clouds was also investigated using the CO data from the ESO SEST (Swedish/ESO Submillimeter Telescope) Key-Program (CO $J = 1 - 0$ and $2 - 1$ lines with $50''$ and $25''$ beam width;[28]) toward 92 and 42 positions in the LMC and SMC, respectively, mostly coincident with IRAS sources; the results were reported in multiple papers, including detailed studies of major star-forming giant molecular clouds (GMCs) and less active cloud complexes in the LMC and small molecular cloud complexes in the SMC (see[29] and references therein). Many other CO studies of individual star-forming regions with SEST in both the LMC and SMC followed (e.g., LMC regions N159W, N113,

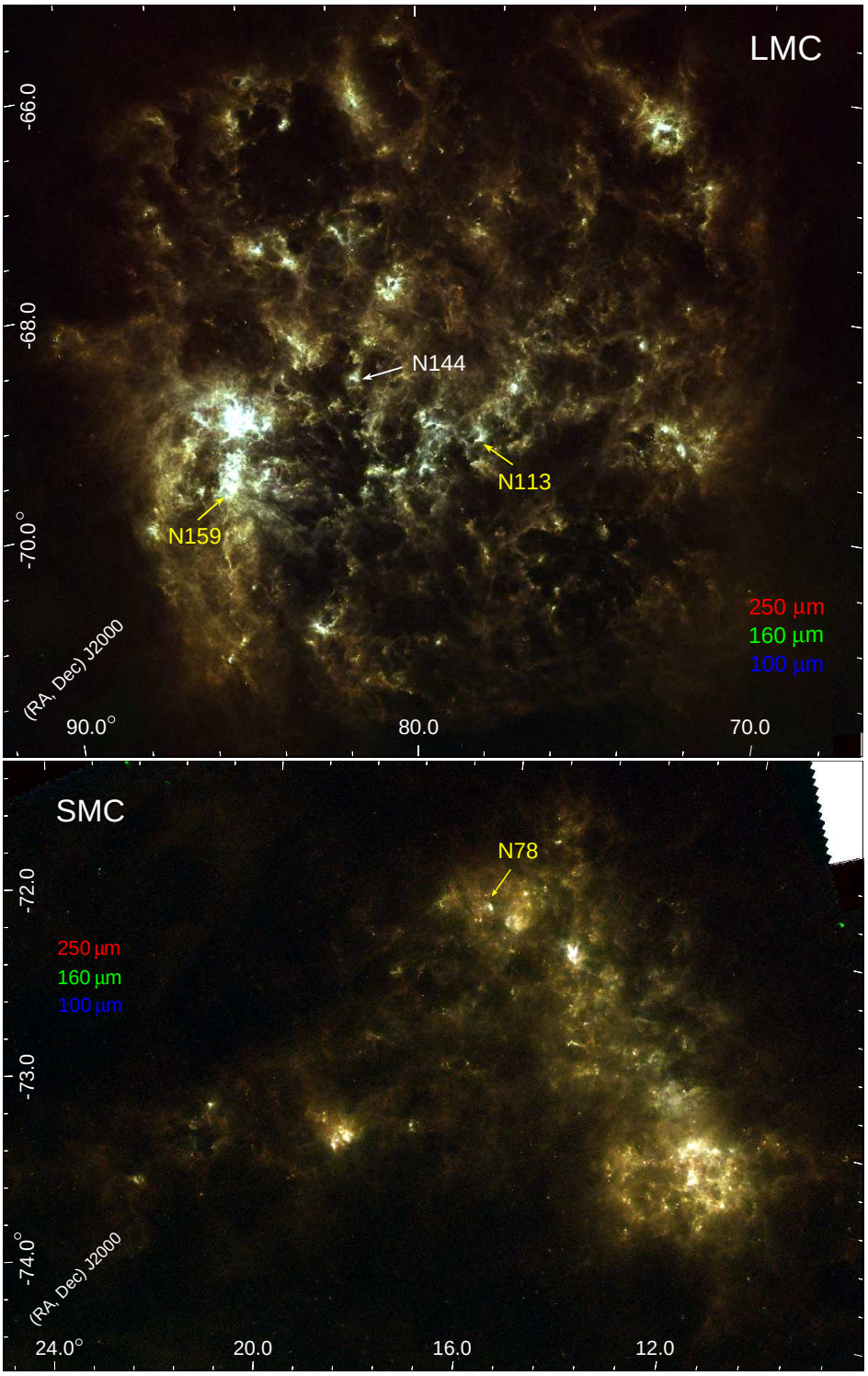

Figure 1: Three-color composite mosaics of the LMC (*top*) and SMC (*bottom*), combining the *Herschel*/HERITAGE 250 μm (red), 160 μm (green), and 100 μm (blue) images.[21] Star-forming regions harboring sources with the detection of COMs (N 113 and N 159 in the LMC and N 78 in the SMC; see Table 2) are indicated with yellow arrows and labeled. The location of the star-forming region N 144 hosting ST 11, a hot core without COMs, is indicated in white. North is up and east to the left.

N44BC, and N214DE[30]).

The first unbiased spectral line survey of an individual star-forming region in the LMC was performed by[31] using SEST and centered on the N 159W molecular peak in N 159 – the brightest NANTEN GMC with H II regions. The observations covered a 215–245 GHz frequency range in several bands and selected bright lines at lower frequencies (∼100 GHz; half-power beam width, HPBW, is ∼23″ at 220 GHz and 50″ at 100 GHz). No COM transitions covered by these observations (e.g., propyne: CH_3CCH $J = 5 - 4$ and $J = 6 - 5$ and CH_3OCH_3 $J = 6 - 5$ lines) were detected.[31] found that fractional abundances with respect to H_2 for molecules detected in N 159W (^{13}CO, $C^{18}O$, CS, SO, HCO^+, HCN, HNC, CN, and H_2CO – formaldehyde) are typically a factor of 10 lower than those observed in the Galaxy.

The multi-region, multi-line SEST 3 mm (85–115 GHz) survey by[32] focused on one SMC (LIRS 36 or N 12) and four LMC (N 113, N 44BC, N 159HW, and N 214DE) molecular cloud cores. They detected the C_2H, HCN, HCO^+, HNC, CS, ^{13}CO, CN, ^{12}CO transitions, but the CH_3OH $J = 2 - 1$ line at ∼96.74 GHz covered by their observations was not detected toward any of the regions. The follow-up study on N 12 in the SMC included the 2, 1.3, and 0.85 mm SEST bands, but also failed to detect CH_3OH or other COMs.[33]

The first detection of a COM in the Magellanic Clouds was reported by[16] in their SEST 0.85, 1.3, 2, and 3 mm survey of the SMC LIRS 49 (or N 27) and LMC 30 Dor–10, 30 Dor–27, N 159W, N 159S, and N 160 regions, covering a range of metallicities and UV radiation strengths. N 159W was the only region where CH_3OH was detected: $J = 2 - 1$ and two $3 - 2$ lines at ∼96.7 and ∼145.1 GHz, respectively (see Table 1). The[16]'s observations covered the $J = 6 - 5$ and $J = 8 - 7$ lines of CH_3CCH, but only marginal ($\sim 2.5\sigma$) detections are reported toward one region – N 159W.[16] estimated the CH_3OH fractional abundance with respect to H_2 of 4.3×10^{-10} in N 159W. The authors indicated that the derived physical and chemical quantities are averages over spatial scales probed by their observations (10–15 pc in the 3 mm, and 5–10 pc in the 2/1.3 mm bands). Overall, the molecular abundances in N 159W

where CH_3OH was detected are typically five to twenty times lower than those measured in the Galactic molecular clouds, assuming that hydrogen is mainly in molecular form within the clouds.[16] concluded that reduced abundances are likely to be a combined effect of lower abundances of carbon and oxygen and higher photodissociation rates of molecules, both due to the lower metallicity in the LMC.

An extensive spectral line study on N 113, previously observed by[32] at 3 mm (see above), provided new detections of CH_3OH.[17] Their SEST observations covered the 0.85, 1.3, 2, and 3 mm bands. The rich spectral line inventory included two $J = 2 - 1$ and two $J = 3 - 2$ lines of CH_3OH (see Table 1). The CH_3OH abundance with respect to H_2 was estimated to be $\sim 5 \times 10^{-10}$, similar to that observed in N 159W by[16], and an order of magnitude lower than that observed in the Galaxy.

N 113 and N 159W remain the best-studied regions in the LMC in terms of chemical inventory. The initial single-dish surveys were followed by interferometric observations with the Australia Telescope Compact Array (ATCA) with 4″–6″ angular resolutions by[34] (N 113 only) and[35] (N 113, N 159, N 105, and N 44) that focused on dense gas tracers such as HCO^+ and HCN.[36] searched for NH_3 $(1,1)$ and $(2,2)$ in seven star-forming regions in the LMC (N 113, N 159W, N 159S, 30 Dor 10, N 44 BC, N 105 A, and N 83 A) with ATCA (HPBW∼9″–17″) and only detected it toward N 159W with an abundance of $\sim 4 \times 10^{-10}$ with respect to H_2 – 1.5–5 orders of magnitude lower than observed in Galactic star-forming regions.

The most recent multi-region, multi-line single-dish survey was conducted by[37] using the Mopra 22-m telescope's 3 mm band (HPBW∼38″ at 90 GHz and 30″ at 115 GHz). The sample included seven H II regions: NQC2, CO Peak 1, N 79, N 44C, N 11B, N 113, and N 159W. That work confirmed lower molecular abundances in the LMC star-forming regions. Those observations failed to detect CH_3OH and other COMs.

The results of the single dish molecular line surveys of individual H II regions in the LMC and SMC indicate a deficiency of CH_3OH in these low-metallicity galaxies. This deficiency is also supported by the low detection rate of CH_3OH masers in the Magellanic Clouds.[38]

Table 1: CH_3OH Transitions Detected in the LMC in Single-Dish Observations[a,b]

Region	Species	Transition	Frequency (GHz)	E_U (K)	Ref.
N 159W	CH_3OH v_t=0[c]	$2_{-1,2}$–$1_{-1,1}$ E	96.739362	12.54	[16]
		$2_{0,2}$–$1_{0,1}$ A^+	96.741375	6.97	[16]
		$2_{0,2}$–$1_{0,1}$ E	96.744550	20.09	[16]
		$2_{1,1}$–$1_{1,0}$ E	96.755511	28.01	[16]
		$3_{-1,3}$–$2_{-1,2}$ E	145.09747	19.51	[16]
		$3_{0,3}$–$2_{0,2}$ A^+	145.10323	13.93	[16]
N 113	CH_3OH v_t=0	$2_{-1,2}$–$1_{-1,1}$ E	96.739362	12.54	[17]
		$2_{0,2}$–$1_{0,1}$ A^+	96.741375	6.97	[17]
		$3_{-1,3}$–$2_{-1,2}$ E	145.09747	19.51	[17]
		$3_{0,3}$–$2_{0,2}$ A^+	145.10323	13.93	[17]

[a] All the observations were conducted with SEST. The SEST's half-power beam sizes are 61″–54″ and 47″–24″ in frequency ranges of 85–98 GHz and 109–219 GHz, respectively (from[17]); [b] The table uses the Cologne Database for Molecular Spectroscopy (CDMS) notation from the National Radio Astronomy Observatory (NRAO) Spectral Line Catalog (Splatalogue). For CH_3OH (N K_a K_c p v), a sign value of K_a is used to differentiate E_1 (+) and E_2 (−) states (both belong to the same E symmetry species); [c] The four transitions at ∼96.7 GHz are blended.

conducted a complete systematic survey for 6668-MHz CH_3OH and 6035-MHz excited-state OH masers in both the LMC and SMC using the Methanol Multibeam (MMB) survey receiver on the 64-m Parkes telescope (HPBW∼3′.3), supplemented by higher sensitivity targeted observations of known star-forming regions. The survey resulted in a detection of only one maser of each kind, increasing the number of known 6668-MHz CH_3OH masers in the LMC to four.[39–41] [42] later detected a single 12.2 GHz CH_3OH maser in the LMC. To date, no CH_3OH masers have been detected in the SMC.[38] estimated that CH_3OH masers in the LMC are underabundant by a factor of ∼45 (or ∼4–5 after correcting for differences in the star formation rates between the galaxies) and interstellar OH and H_2O masers by a factor of ∼10 compared to the Galaxy.

The *Spitzer Space Telescope* (*Spitzer*;[43]) and *Herschel Space Observatory* (*Herschel*;[44]) enabled studies of young stellar object (YSO) populations in the LMC and SMC, both galaxy-wide and in individual star-forming regions. Using the data from the "*Spitzer* Surveying the Agents of Galaxy Evolution" (SAGE;[45]) and "Surveying the Agents of Galaxy Evolution in

the Tidally Stripped, Low Metallicity Small Magellanic Cloud" (SAGE-SMC;[46]), thousands of YSOs were identified in the Magellanic Clouds, dramatically increasing the number of previously known YSOs (from 20/1 in the LMC/SMC; e.g.,[47–52]). YSOs detected by *Spitzer* include mostly Stage I (protostars with accreting envelopes and disks) and also Stage II (disk-only) YSOs; the youngest Stage 0/I YSOs (protostars in the main accretion stage) were identified with *Herschel* using the data from the "HERschel Inventory of The Agents of Galaxy Evolution" (HERITAGE,[21]; e.g.,[53,54]) survey. The *AKARI* Large-area Survey of the Large Magellanic Cloud (LSLMC) also carried out near- to mid-infrared photometric survey and near-infrared slitless spectroscopic survey towards the LMC, whose datasets also are used to search for YSOs in the LMC.[55–57] On a galaxy-wide scale, YSO lists can be utilized to determine a star formation rate in each galaxy. On scales of individual star-forming clouds, YSO catalogs can also be used to study star formation rate, star formation efficiency, the evolutionary stage of the GMCs, and provide targets for follow-up detailed observations.

Spectroscopic follow-up observations of *Spitzer*, *Herschel*, and *AKARI* YSOs in the LMC and SMC revealed chemical differences in the YSO envelopes between these galaxies and compared to Galactic YSOs, which can be explained as a consequence of differences in metallicity (see Section 3).

3 Near- to Mid-Infrared Spectroscopy: More Evidence for Chemical Differences between the LMC, SMC, and the Milky Way

The mid-IR studies on the LMC YSOs with *Spitzer* Infrared Spectrograph (IRS)[11,58–60] and near-IR studies with the AKARI satellite[61,62] and ground-based instrumentation[11,59] found differences in ice chemistry between the LMC and the Galaxy. In cold molecular clouds, layers of ice form on the surface of dust grains. The main constituent of ice in envelopes of

YSOs is H_2O, mixed primarily with CO and CO_2.[63] Since the H_2O ice abundances ($\sim 10^{-4}$; e.g.,[64,65]) exceed by a few orders of magnitude the gas-phase abundances, understanding gas–grain processes is crucial to fully understand the chemistry in the YSO envelopes.

In the LMC and by comparison to Galactic samples, CO_2 ice column densities are enhanced with respect to H_2O ice[58,60,62], while relative CO-to-CO_2 abundances are unchanged.[11 11] proposed the scenario where the high CO_2/H_2O ratio is due to the low abundance of H_2O in the LMC. If there is a difference in the optical extinction A_V threshold for H_2O and CO_2 ices (as the observations suggest), there could be an envelope of less shielded material that shows H_2O ice but no CO_2 ice. The strong interstellar radiation in the LMC penetrates deeper into the YSO envelopes as compared with Galactic YSOs, possibly destroying H_2O ice in less-shielded outer layers without affecting CO_2 and H_2O ice mixtures that exist deeper in the envelope.

In their Very Large Telescope (VLT)'s Infrared Spectrometer And Array Camera (ISAAC) near-IR spectroscopic observations,[66] marginally detected CH_3OH ice absorption band toward two embedded massive YSOs in the LMC with the abundances suggesting that solid CH_3OH is less abundant for high-mass YSOs in the LMC than those in the Galaxy. They proposed a model which explains both the low abundance of CH_3OH and the higher abundance of solid CO_2 found in previous studies. In this "warm ice chemistry" model, the grain surface reactions at a relatively high temperature ($T \gtrsim 20$ K) are responsible for the observed characteristics of ice chemical composition in the LMC. The high dust temperature in the low-metallicity environment caused by the strong interstellar radiation field leads to inefficient H atom sticking and CO hydrogenation to CH_3OH on grain surfaces. At the same time, the production of CO_2 is enhanced as a result of the increased mobility of parent species (CO and OH; see Section 5.2.1 for a discussion on theoretical models).

The *Spitzer*/IRS spectroscopy also revealed several COMs in the *circumstellar* environment of SMP LMC 11 (or LHA 120–N 78) - an object in the LMC classified as a carbon-rich planetary nebula (PN) in the optical, but with infrared properties consistent with

it being in the transition from the post-asymptotic giant branch (AGB) to the PN stage (e.g.,[67] and references therein).[67] identified the diacetylene (C_4H_2), ethylene (C_2H_4), triacetylene (C_6H_2), benzene (C_6H_6), and possibly methylacetynele (CH_3C_2H; commonly known as propyne which is found also in Titan's atmosphere) absorption bands in the *Spitzer*/IRS spectrum of SMP LMC 11. C_6H_6 is a simplest building block of polycyclic aromatic hydrocarbons (PAHs), which are abundant and ubiquitous in the interstellar medium (e.g.,[68]). In the subsequent analysis and modeling of the same *Spitzer*/IRS spectrum,[69] questioned the detection of C_6H_2, but confirmed the detection of CH_3C_2H. SMP LMC 11 shows a peculiar chemistry, not typical for PN or post-AGB objects in general, e.g., it is one of only two evolved stars in which hydrocarbons up to benzene in absorption are detected (e.g.,[69–71]).

4 The Quest for Detecting COMs in the Magellanic Clouds with ALMA

The detection of CH_3OH and more complex molecules in the Magellanic Clouds has been accelerated by the advent of ALMA. ALMA provides high spatial resolution and sensitivity which enabled studies in the LMC/SMC that in the pre-ALMA era were only possible in our Galaxy. The wide frequency coverage of ALMA observations (up to four ∼2 GHz spectral windows in the submm/mm wavelength range) allows for simultaneous observations of multiple molecular species and enables serendipitous discoveries.

4.1 Hot Core without COMs: LMC ST 11

ST 11 is a high-mass YSO (∼5×10^5 $L_\odot$, *Spitzer* YSO 052646.61−684847.2;[47,48,54,62,72], or IRAS 05270–6851) located in the N 144 star-forming region in the LMC (Fig. 1). In the pre-ALMA era, the spectral properties of the source were well studied with mid-infrared and near-infrared spectroscopy, which have detected absorption bands due to H_2O ice, CO_2 ice, and silicate dust, as well as emission due to Polycyclic Aromatic Hydrocarbon (PAH) and

hydrogen recombination lines.[62,72]

The high-resolution (∼0.″5 or ∼0.12 pc) submillimeter (∼0.86 mm) observations toward ST 11 with ALMA revealed the presence of a hot molecular core associated with the source.[73] According to the rotational diagram analysis of multiple $^{32}SO_2$ and $^{34}SO_2$ lines, the gas temperature of the hot core region is estimated to be ∼100–200 K. The total gas density of the source is estimated to be higher than 2×10^6 cm^{-3} based on the analysis of the submillimeter dust continuum. Emission lines of CO, $C^{17}O$, HCO^+, $H^{13}CO^+$, H_2CO, NO, H_2CS, ^{33}SO, $^{33}SO_2$, and SiO are also detected from the compact region associated with the source. High-velocity components are detected in the line profile of CO (3–2), which suggests the presence of molecular outflow in this source.

CH_3OH and larger COMs are not detected toward ST 11, despite the high gas temperature that is sufficient for the ice sublimation and despite the detection of H_2CO, a small organic molecule. The estimated upper limit on the CH_3OH gas fractional abundance of 8×10^{-10} is significantly lower than those of Galactic hot cores by a few orders of magnitude ([73], see Table 3).[73] hypothesized that the inhibited formation of CH_3OH on the dust surface before the hot core stage could be responsible for this deficiency.[73] also estimated upper limits on fractional abundances with respect to H_2 for (CH_3OCH_3, $HCOOCH_3$, C_2H_5OH) of ($<1.5\times10^{-8}$, $<1.8\times10^{-8}$, $<3.7\times10^{-9}$). These upper limits indicate that in ST 11 the fractional abundance of CH_3OCH_3 is at least an order of magnitude lower compared to Galactic hot cores, while the $HCOOCH_3$ and C_2H_5OH fractional abundances are comparable to the average abundances observed in the Galactic counterparts.

4.2 Cold Methanol: LMC N159W–South and SMC IRAS 01042−7215

4.2.1 N159W–South

The N 159 star-forming region located south from 30 Doradus is one of the best studied areas in the LMC hosting H II regions, young stellar clusters, *Spitzer* and *Herschel* massive YSOs, and a water maser (e.g.,[49] and references therein;[42]). As described in Section 2,

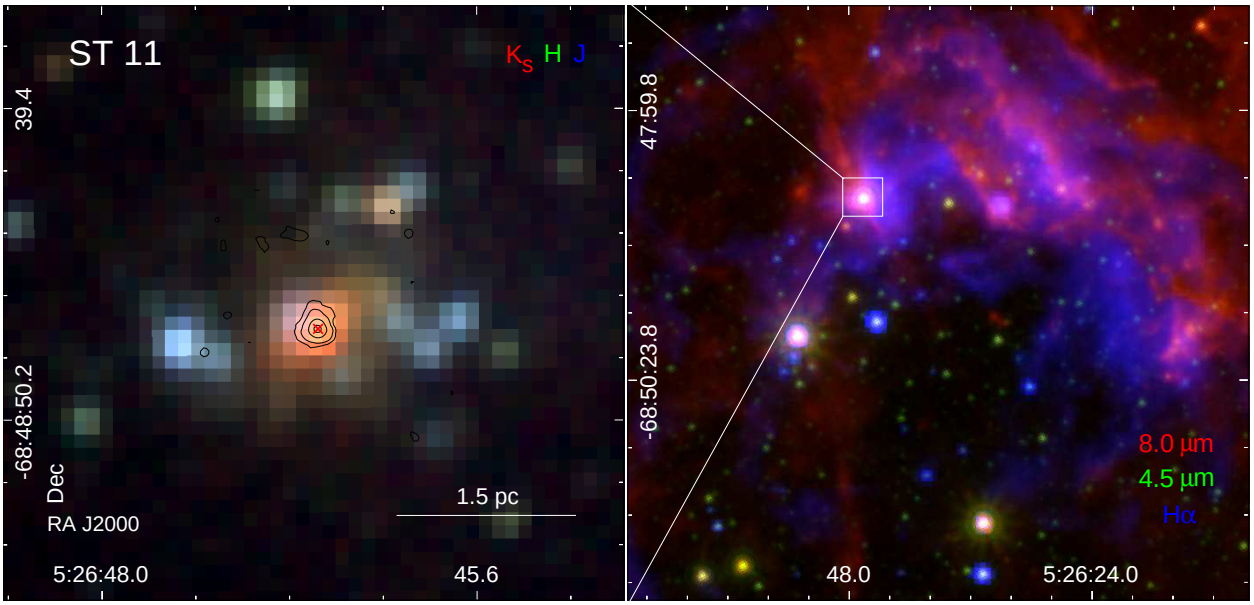

Figure 2: *Left:* A three-color mosaic combining the InfraRed Survey Facility (IRSF) K_s (red), H (green), and J (blue;[74]) images for the LMC source ST 11 – the source with a hot core chemistry, but no COMs detection.[73] *Right:* a three-color mosaic combining the *Spitzer*/SAGE 8.0 μm (red), 4.5 μm (green;[45]), and the MCELS Hα (blue;[75]) images. The ALMA 840 μm continuum contours are overlaid on the image in the left panel; the contour levels are (3, 6, 20, 40) $\times$ 0.94 mJy beam^{-1}, the 840 μm image rms noise level. The ALMA beam size is $0\farcs5 \times 0\farcs5$. The red '$\times$' symbol in the left panel indicates the position of the *Spitzer* YSO – the bright source in the mosaic shown in the right panel.

N 159 was the target of detailed spectral line observations with single-dish telescopes. It is the brightest region in the LMC in ^{12}CO at SEST/Mopra resolution. One of the three giant molecular clouds in N 159, N 159W, is one of only two regions with a CH_3OH detection in the pre-ALMA era.

The first high-resolution ($\sim$1$''$ or $\sim$0.25 pc) ^{13}CO and ^{12}CO (2–1) ALMA observations of N159W resolved the molecular gas emission into filaments and detected two sources with outflows.[77] It was the first detection of both filamentary structure and outflows outside the Galaxy. These observations identified two main regions of high-mass star formation which were dubbed N 159W–North and N 159W–South (or N 159W–N and N 159W–S, respectively). Both N 159W–N and N 159W–S are associated with *Spitzer*/*Herschel* YSOs.[47–49,51,54] Two Stage 0/I YSOs with outflows have masses >30 $M_\odot$ and are associated with 1.3 mm continuum peaks, one in each N 159W–N (YSO–N or *Spitzer* 053937.56−694525.4) and N 159W–

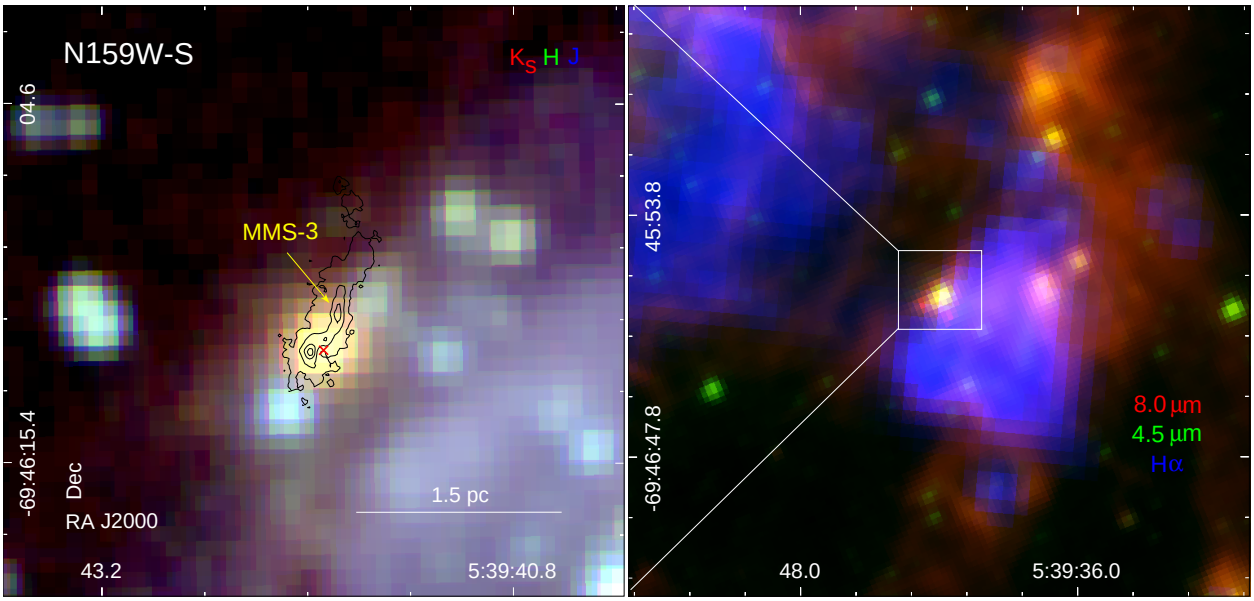

Figure 3: The same as Fig.2, but for N159W–S – the source with a cold methanol detection (PI Peter Schilke, see Sections 4.2.1 and A.1). The ALMA 1.3 mm continuum contours are overlaid on the image in the left panel; the contour levels are (0.1, 0.3, 0.5, 0.7) mJy beam^{-1}, the image rms noise level is 0.027 mJy beam^{-1}.[76] The ALMA beam size is $0\farcs26 \times 0\farcs23$.

S (YSO–S or *Spitzer* 053941.89−694612.0; e.g.,[49]). Based on the kinematics of the molecular gas and the location of YSO–S at the intersection of two ^{13}CO filaments,[77] proposed that star-formation in N 159W–S was triggered by the collision of two filaments $\sim 10^5$ years ago.

This model was revised by[76] based on the four times higher resolution observations of CO isotopes ($\sim 0\farcs25$ or 0.06 pc), which resolved the filaments in N 159W–S into a complex, hub–filament structure. Multiple protostellar sources with outflows separated by 0.2–2 pc were detected along the main massive filament. They correspond to the three major 1.3 mm continuum peaks dubbed MMS–1, MMS–2, and MMS–3 (see Fig. 5). The[76]'s observations are consistent with a scenario that a large-scale (>100 pc), rather than local ($\sim$10 pc;[77]), collision triggered the formation of both filaments and massive protostars in N 159W–S.

MMS–1 and MMS–2 continuum sources are associated with two near-infrared sources N 159 A7 '121' and '123', respectively, detected by[78] using high-resolution ($\sim 0\farcs2$) *VLT*/NACO observations. The position of the *Spitzer* YSO (YSO–S in[77]; see Fig. 3) is offset to the west hinting at the possibility that a cluster is being formed. No infrared source is detected to-

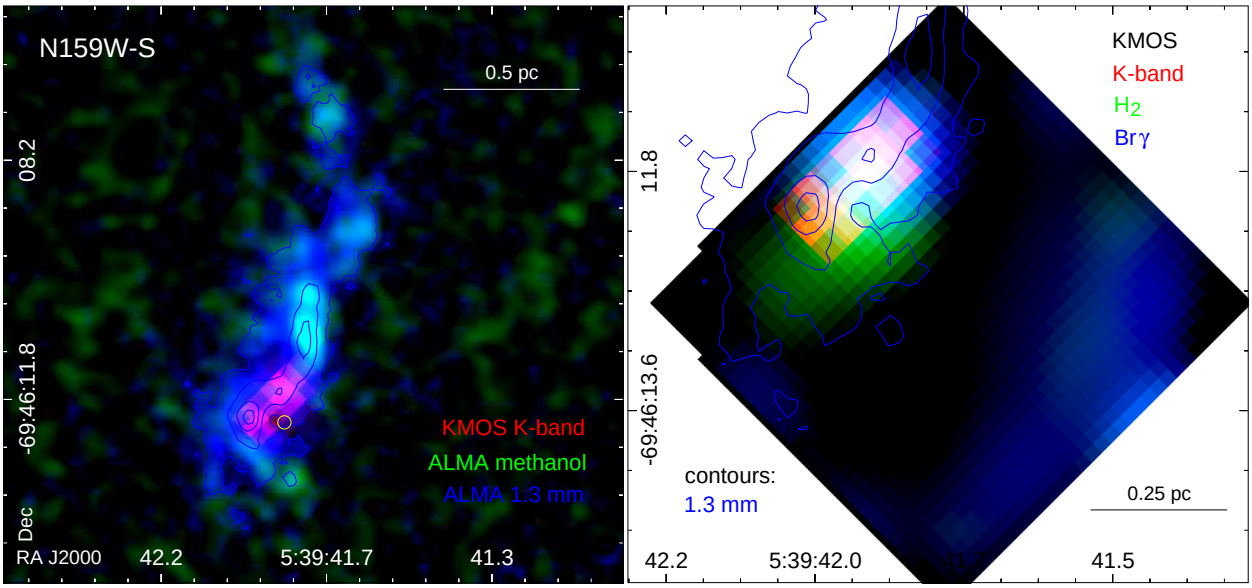

Figure 4: *Left*: Three-color mosaic combining the *VLT*/KMOS *K*-band (red), ALMA CH_3OH (green), and ALMA 1.3 mm (blue) images of N 159W–S. The contours correspond to the 1.3 mm continuum emission with contour levels the same as in Fig. 3. The yellow circle shows the catalog position of the *Spitzer* YSO.[48] *Right*: Three-color mosaic combining KMOS images: *K*-band (red), H_2 (green), and Brγ (blue). The 1.3 continuum contours (the same as in the left panel) are overlaid for reference.

ward MMS–3, indicating that it is the youngest of the three protostars. Recent *VLT*/KMOS observations (a pixel scale 0.″2, a full width at half maximum seeing ∼0.″4; PI Jacob Ward, see Section A.2 for technical details) targeting YSO–S (see Fig. 3) detected the *K*-band continuum, the Brackett-gamma emission line of hydrogen (Brγ), and the H_2 emission line toward N 159 A7 121 (MMS–1) and 123 (MMS–2). As the H_2 and Brγ lines trace shocks and accretion, respectively, they can shed light on the nature of the sources and thus possible formation scenarios of COMs (e.g., non-thermal origin in shocks traced by H_2). The right panel in Fig. 4 shows a combination of the three KMOS images with the ALMA continuum contours overlaid for reference. The extended H_2 emission is associated with outflows from N 159 A7 121 (MMS–1) and 123 (MMS–2) detected by[76] with ALMA. The Brγ emission is only detected toward N 159 A7 123 (MMS–2).

The most recent ALMA observations of N 159W–S detected multiple CH_3OH peaks throughout the region (see Fig. 5; PI P. Schilke) with the brightest emission associated

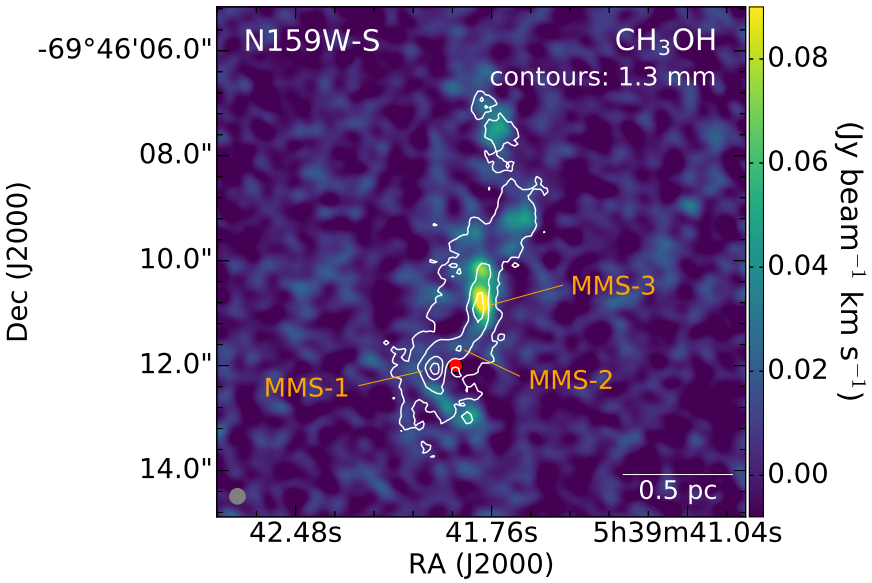

Figure 5: The integrated intensity image of CH_3OH for N 159W–S with the 1.3 mm continuum contours and the positions of the continuum peaks (MMS–1, MMS–2, and MMS–3;[76]) overlaid. The position of the *Spitzer* YSO is indicated with the red filled circle (e.g.,[49]). The 1.3 mm continuum contour levels and the ALMA beam size are the same as in Fig. 3. The ALMA synthesized beam size of the CH_3OH observations (shown in the lower left corner) is $0\farcs3 \times 0\farcs3$.

with the continuum source MMS–3. The left panel in Fig. 4 shows a three-color mosaic combining the KMOS *K*-band, ALMA CH_3OH and 1.3 mm continuum emission. No CH_3OH emission is detected toward MMS–1 and MMS–2 that have infrared counterparts. Although these observations were designed to detect multiple COMs (e.g, CH_3OH, CH_3CN – methyl cyanide, $HCOOCH_3$, CH_3OCH_3), only CH_3OH was found. The detection of multiple peaks hints at the possibility that there is an underlying more extended distribution of CH_3OH that is resolved out.

Preliminary Local Thermodynamic Equilibrium (LTE) fitting using multiple CH_3OH lines (∼241.7–241.9 GHz; see Table 5) detected toward the two brightest peaks indicate that the gas is cold (∼14 K). Methanol forms on grain surfaces and has to be released to the gas phase by energetic events to be detectable. The desorption mechanisms include sublimation by infrared heating by a forming star, photodesorption by UV photons, sputtering by shocks, and chemical desorption (see a discussion in Section 5). None of these mechanisms is directly

supported by the observations of N 159W–S: the gas is cold (desorption by the infrared and UV heating is less likely) and the line widths are narrow (broad lines are expected in the shock sputtering scenario). Moreover, the average cosmic ray flux in the LMC is low, making the cosmic ray induced UV radiation less effective than in the Galaxy. Since the analysis of the ALMA CH_3OH data is preliminary, we do not provide physical parameters for N159W–S in Table 2.

4.2.2 IRAS 01042−7215

IRAS 01042–7215 is a high-mass YSO ($\sim 2\times10^4$ $L_\odot$; e.g.,[11,79]; *Spitzer* YSO SSTISAGEMA J010549.30–715948.5,[52]) located in the northeast region of the SMC bar at the outskirts of the N 78 star-forming region (see Figs. 1 and 6). The source is well studied through near-infrared and mid-infrared spectroscopy; absorption bands due to H_2O ice, CO_2 ice, and silicate dust are detected, while prominent PAH bands and ionized metal lines are not detected.[10,11,59,79] No CH_3OH ice has been detected toward IRAS 01042–7215.

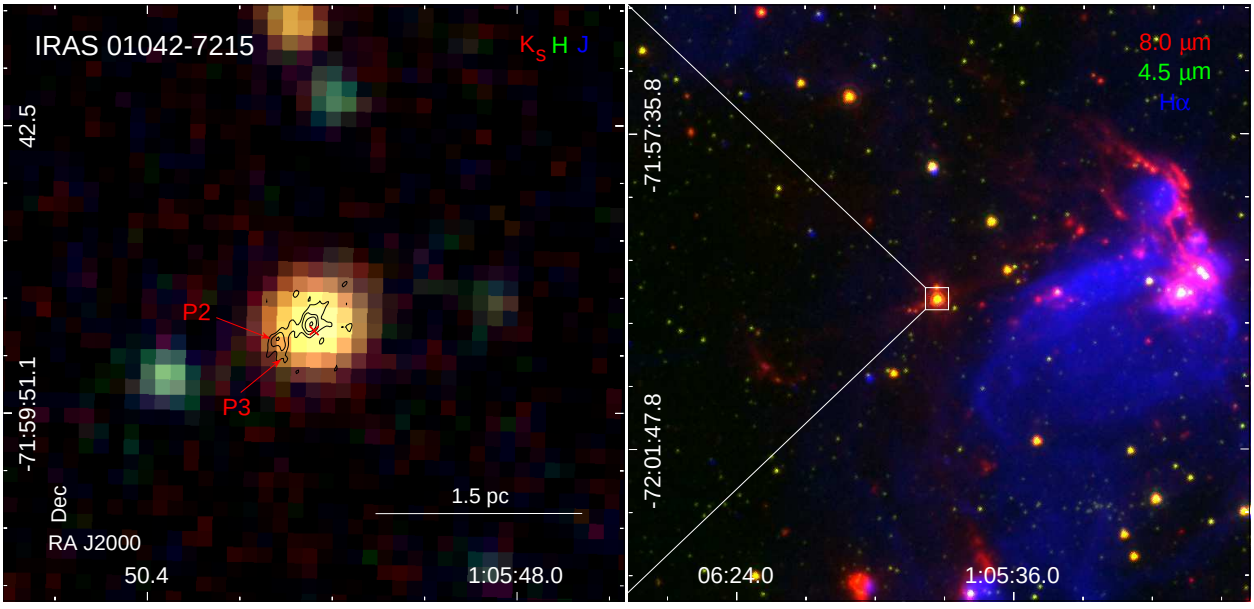

Figure 6: The same as Fig.2, but for the field around the SMC source IRAS 01042−7215 where CH_3OH was detected toward sources P2 and P3 (indicated in the left panel) corresponding to the CH_3OH peaks.[19] The ALMA 1.2 mm continuum contours are overlaid. The continuum contour levels are (3, 6, 10, 20) × 21 mJy beam^{-1}, the 1.2 mm image rms noise level. The ALMA synthesized beam size is 0.″35 × 0.″22.

Recent *VLT*/SINFONI *K*-band observations (a pixel scale of 0.″1, a full width at half maximum seeing ∼0.″6;[80]) detected the Brγ and H_2 emission lines towards IRAS 01042−7215.[80] Figure 7 shows a three-color mosaic combining the SINFONI *K*-band continuum, H_2, and Brγ images. The SINFONI image reveals a single compact embedded source ($A_v = 16 \pm 8$ mag) with little or no extended line emission. The measured H_2 emission line ratios are consistent with expectations for shocked emission.[81]

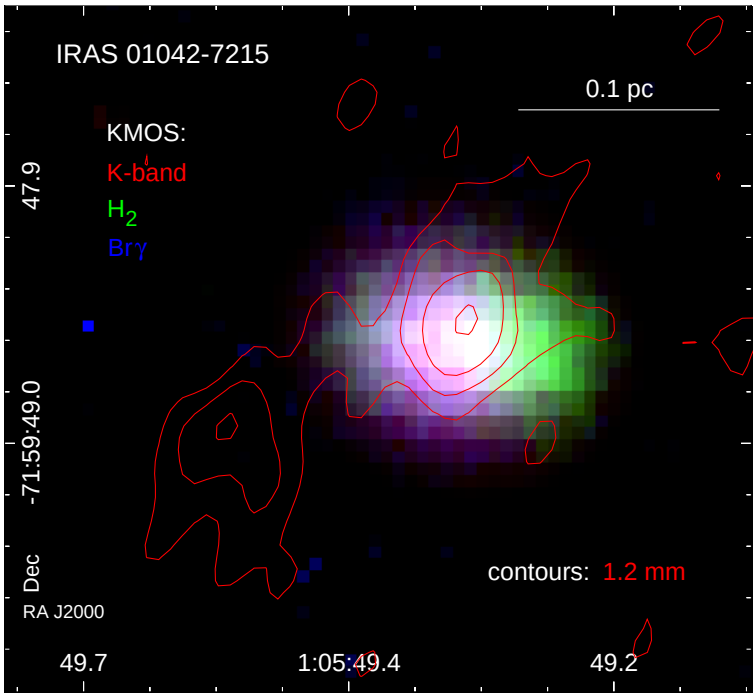

Figure 7: Three-color mosaic of the IRAS 01042–7215 field combining the *VLT*/SINFONI *K*-band (red), H_2 (green), and Brγ (blue) images.[80] Red contours correspond to the ALMA 1.2 mm continuum emission with contour levels the same as in Fig. 6.

The high-resolution (∼0.″22–0.″37 or ∼0.07–0.11 pc at the distance of the SMC) 1.2 mm ALMA observations detected two continuum peaks – 'P1' and 'P2/P3' toward IRAS 01042–7215. P2/P3 is further resolved into two sources (P2 and P3) corresponding to the CH_3OH emission peaks where multiple CH_3OH transitions are detected (Fig. 8;[19]).

The 1.2 mm continuum source P1 is associated with the high-mass YSO corresponding to the IRAS source, while no infrared sources are detected at the positions of P2 and P3 (see Fig. 7 and[19]). P2 and P3 correspond to the two CH_3OH emission peaks in the region; no

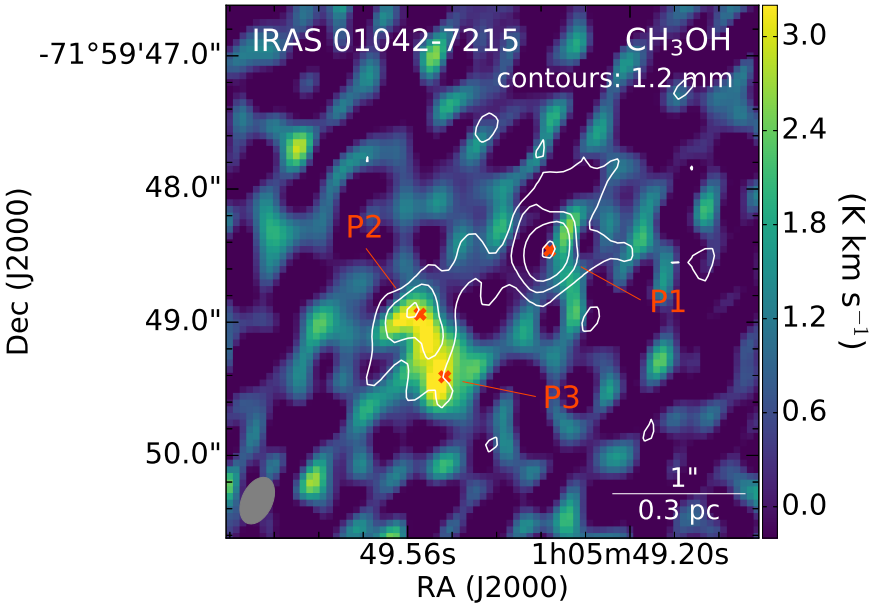

Figure 8: The CH_3OH integrated intensity image (the average of the CH_3OH $5_{-1,5} - 4_{-1,4}$ E and $5_{0,5} - 4_{0,4}$ A^+ lines) of IRAS 01042−7215 in the SMC. The 1.2 mm continuum contours are overlaid; the contour levels and the size of the ALMA synthesized beam shown in the lower left corner are the same as in Fig. 6.

CH_3OH is detected toward P1 (Fig. 8 and[19]). Besides CH_3OH, CS, $C^{33}S$, SO, SO_2, $H^{13}CO^+$, $H^{13}CN$, SiO are detected toward P2/P3, but no COMs larger than CH_3OH.

The rotation diagram analysis of the CH_3OH lines for IRAS 01042–7215 P2 and P3 suggests that the temperature of the CH_3OH gas is low (∼20 K), well below the sublimation temperature of the CH_3OH ice (∼80 K;[82]). This is another example of a source in the Magellanic Clouds with the detection of 'cold methanol'. The CH_3OH abundances relative to H_2 for P2 and P3 are an order of magnitude lower than those for hot cores A1 and B3 in N 113 (see Table 2 and Section 4.3). The origin of CH_3OH gas in P2/P3 is still under debate.[19] suggest that a possible origin could be sputtering of the ice mantles by shocks triggered by the outflow from nearby YSOs, or chemical desorption of CH_3OH from dust surfaces. The presence of shocked but cold CH_3OH gas has been suggested in Galactic infrared dark clouds, indicating that CH_3OH may be tracing relatively old shocks (e.g.,[83]).

Table 2: Positions, Physical Properties, and Fractional Abundances for Sources Described in Section 4 with COMs Detection or Measured Upper Limits with ALMA

Source	R.A. (J2000) (h m s)	Decl. (J2000) (° ′ ″)	Molecule	$T_{\rm rot}$ (K)	N (cm^{-2})	$N/N(H_2)$	Type[m]	Ref.
			LMC					
N 113 A1[a]	05:13:25.17	−69:22:45.5	CH_3OH[g]	134±6	$(1.6\pm0.1)\times10^{16}$	$(2.0\pm0.3)\times10^{-8}$	HC	18
			CH_3OCH_3	.....[h]	$(1.8\pm0.5)\times10^{15}$	$(2.2\pm0.7)\times10^{-9}$		
			$HCOOCH_3$	.....[h]	$(1.1\pm0.2)\times10^{15}$	$(1.4\pm0.4)\times10^{-9}$		
N 113 B3[a]	05:13:17.18	−69:22:21.5	CH_3OH[g]	131±15	$(6.4\pm0.8)\times10^{15}$	$(9.1\pm1.7)\times10^{-9}$	HC	18
			CH_3OCH_3	.....[h]	$(1.2\pm0.4)\times10^{15}$	$(1.7\pm0.7)\times10^{-9}$		
			$HCOOCH_3$[f]	.....[h]	$< 3.4\times10^{15}$	$< 0.5\times10^{-9}$		
N159W–South[b,j]	05:39:41	−69:46:06	CH_3OH	.....	.....	.....	CM	[k]
ST 11[c,i]	05:26:46.60	−68:48:47.03	CH_3OH	100[l]	$< 3.5\times10^{14}$	$< 8\times10^{-10}$	HC*	73
			CH_3OCH_3	100[l]	$< 1.3\times10^{15}$	$< 3\times10^{-9}$		
			$HCOOCH_3$	100[l]	$< 7.1\times10^{15}$	$< 2\times10^{-8}$		
			C_2H_5OH	100[l]	$< 2.2\times10^{15}$	$< 5\times10^{-9}$		
			SMC					
IRAS 01042−7215 P2[d,i]	01:05:49.54	−71:59:48.94	CH_3OH	18±5	$(1.4^{+1.1}_{-0.6})\times10^{14}$	$(5.0^{+4.2}_{-2.3})\times10^{-10}$	CM	19
IRAS 01042−7215 P3[e,i]	01:05:49.50	−71:59:49.41	CH_3OH	22±6	$(1.6^{+1.1}_{-0.6})\times10^{14}$	$(1.5^{+1.0}_{-0.6})\times10^{-9}$	CM	19

[a] The positions of N 113 A1 and B3 correspond to the ∼224.3 GHz continuum peaks; [b] Multiple CH_3OH peaks are detected across the N159W–South molecular clump (see Section 4.2.1 and Fig. 5); [c] The position of ST 11 corresponds to the 359 GHz continuum peak; [d] The position of IRAS 01042−7215 P2 corresponds to the $C^{33}S$, H_2CS, and SiO peak; [e] The position of IRAS 01042−7215 P3 corresponds to the CH_3OH peak; [f] a tentative detection; [g] $T_{\rm rot}$ and N were determined using the MADCUBAIJ software with the initial estimates based on the rotational diagram analysis of CH_3OH; [h] $T_{\rm rot}$ for CH_3OCH_3 and $HCOOCH_3$ was assumed to be equal to $T_{\rm rot}$ determined for CH_3OH[18]; [i] $T_{\rm rot}$ and N were determined based on the rotational diagram of CH_3OH; the values presented in the table are the revised values from[19] based on new ALMA observations (PI T. Shimonishi); [j] The analysis of the N159W–South data is preliminary, thus we do not provide physical parameters for this region; [k] PI P. Schilke; [l] The average rotation temperature of SO_2, $^{34}SO_2$, and $^{33}SO_2$; N and $N/N(H_2)$ upper limits are at the 2σ level; [m] Type: HC – a hot core; HC* – a hot core with no COMs; CM – a source with cold methanol.

4.3 Hot Cores with COMs More Complex than Methanol: LMC N 113 A1 and B3

To date, COMs with more than six atoms have only been reliably detected in the Magellanic Clouds toward two sources, both in the LMC N 113 star-forming region. The physical and chemical characteristics of N 113 make it one of the most interesting star-forming regions in the LMC. Like N 159, it was the target of detailed spectral line studies with single-dish telescopes (see Section 2) that resulted in the detection of CH_3OH.[17]

N 113 contains: (1) one of the most massive ($\sim 10^5$ $M_\odot$) and richest GMCs in the LMC[27]; (2) signatures of both recent (Hα emission) and ongoing (e.g., maser and bright IR emission) star formation[34,84]; (3) signatures of star formation triggered by winds from massive stars; (4) the largest number of H_2O and OH masers and the brightest H_2O maser in the entire LMC[38,42,84–86]; (5) and it has among the highest concentrations of *Spitzer*/*Herschel* Stage 0–II YSO candidates in the LMC.[47,48,51,53,54]

Mid-IR sources, maser emission, and compact H II regions in the central part of the GMC associated with the extended gas and dust emission, reveal sites of the current star formation in N 113 (see Fig. 9). The *Spitzer* (3.6–160 μm) and *Herschel* (160–500 μm) images with resolutions ranging from $\sim 2''$ to $38''$ show that this region is dominated by three bright sources, which were identified as 30–40 $M_\odot$ Stage I YSOs (YSO–1, YSO–3, and YSO–4 in Fig. 9: *Spitzer* sources 051317.69−692225.0, 051325.09−692245.1, and 051321.43−692241.5, respectively;[48]) and are characterized by distinct physical conditions ([48,87]; J. M. Oliveira, in prep.).

Detailed *Spitzer* and *Herschel* studies on the YSO population in N 113 were followed by ALMA Band 6 ($\sim$1.3 mm) observations at $\sim$0.18 pc (or $\sim 0\farcs8$) resolution in the molecular transitions that probe a wide density range (10^2–10^7 cm^{-3}) to study both the dense clumps/cores and the lower density gas in the inter-clump regions. The ionized gas and outflow tracers were also included in the program. These observations resulted in a serendipitous discovery of COMs methanol (CH_3OH), methyl formate ($HCOOCH_3$), and dimethyl ether

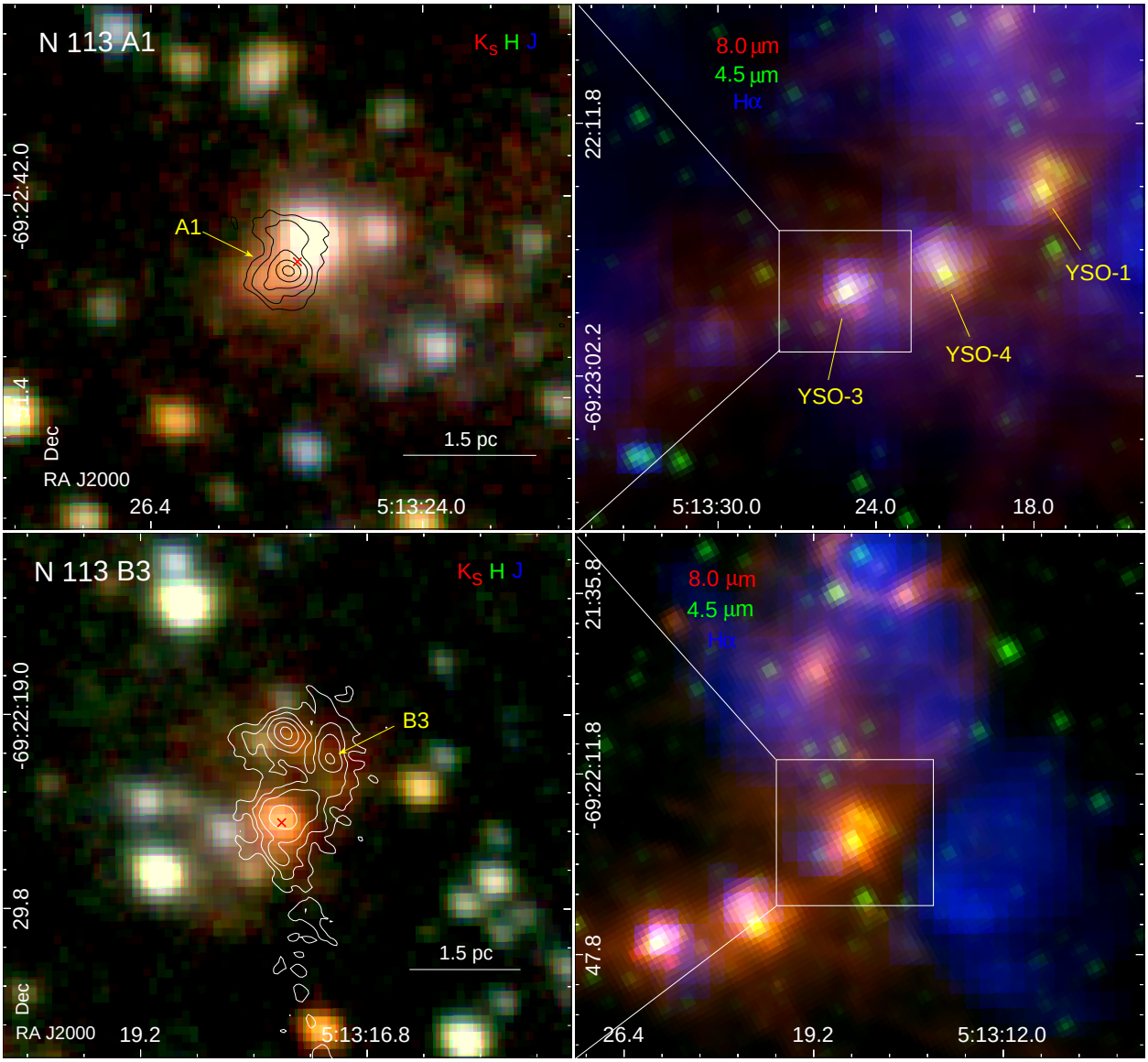

Figure 9: *Left:* The same as in Fig. 2, but for N 113 A1 (*top*) and B3 (*bottom*) hot cores. The contours in the left panel correspond to the 1.3 mm continuum emission.[18] The contour levels are (5, 10, 20, 50) × the image rms noise level of 0.1 mJy beam^{-1}.

(CH_3OCH_3) toward two locations in the region ([18]; see Figs. 9–10). The detected transitions are listed in Table 5. This was the first conclusive detection of COMs more complex than methanol outside the Galaxy and in a low-metallicity environment. COMs were detected toward two 1.3 mm continuum sources 'A1' and 'B3' in the field around *Spitzer* YSO–3 ('Region A' in[18]) and YSO–1 ('Region B'). Figure 9 shows three-color mosaics covering A1 and B3 combining near-infrared bands with 1.3 mm contours overlaid, as well as a larger scale environment in N 113 traced by the *Spitzer* 4.5 and 8.0 μm, and Hα emission. Figure 10 shows the integrated intensity CH_3OH, CH_3OCH_3, and $HCOOCH_3$ images of Regions A and B.

A1 and B3 are compact (diameter $D \sim 0.17$ pc) and are associated with H_2O (A1 and B3) and OH (A1) masers. H_2 column densities of $(8.0 \pm 1.2) \times 10^{23}$ cm^{-2} and $(7.0 \pm 0.9) \times 10^{23}$ cm^{-2} and number densities of $\sim$1.6$\times$10^6 cm^{-3} and $\sim$1.4$\times$10^6 cm^{-3} for A1 and B3, respectively, were estimated using the 1.3 mm continuum data. The LTE analysis of six CH_3OH transitions resulted in rotational temperatures and total column densities ($T_{\rm rot}$, $N_{\rm rot}$) of $(134 \pm 6$ K$, 1.6 \pm 0.1 \times 10^{16}$ cm$^{-2})$ and $(131 \pm 15$ K$, 6.4 \pm 0.8 \times 10^{15}$ cm$^{-2})$ for A1 and B3, respectively.[18] These sizes, number and column densities, and temperatures of A1/B3 are consistent with classic hot cores observed in the Galaxy. COMs emission and association with masers are also among the main characteristics of hot cores. These are the first bona fide detections of complex hot core chemistry outside the Galaxy.

The (CH_3OH, CH_3OCH_3, $HCOOCH_3$) column densities are $(16 \pm 1, 1.8 \pm 0.5, 1.1 \pm 0.2) \times 10^{15}$ cm^{-2} for A1 and $(6.4 \pm 0.8, 1.2 \pm 0.4, < 0.34) \times 10^{15}$ cm^{-2} for B3. Column densities for $HCOOCH_3$ and CH_3OCH_3 were estimated using the same $T_{\rm rot}$ as for CH_3OH, assuming that these molecular species are located in the same region as CH_3OH in A1 and B3.

The (CH_3OH, CH_3OCH_3, $HCOOCH_3$) fractional abundances with respect to H_2 are $(20 \pm 3, 2.2 \pm 0.7, 1.4 \pm 0.4) \times 10^{-9}$ for A1 and $(9.1 \pm 1.7, 1.7 \pm 0.7, < 0.5) \times 10^{-9}$ for B3 (see Table 2). The CH_3OH fractional abundances in A1/B3 are over an order of magnitude larger than an upper limit estimated for ST 11 by[73] (see Section 4.1). Table 3 lists CH_3OH, CH_3OCH_3,

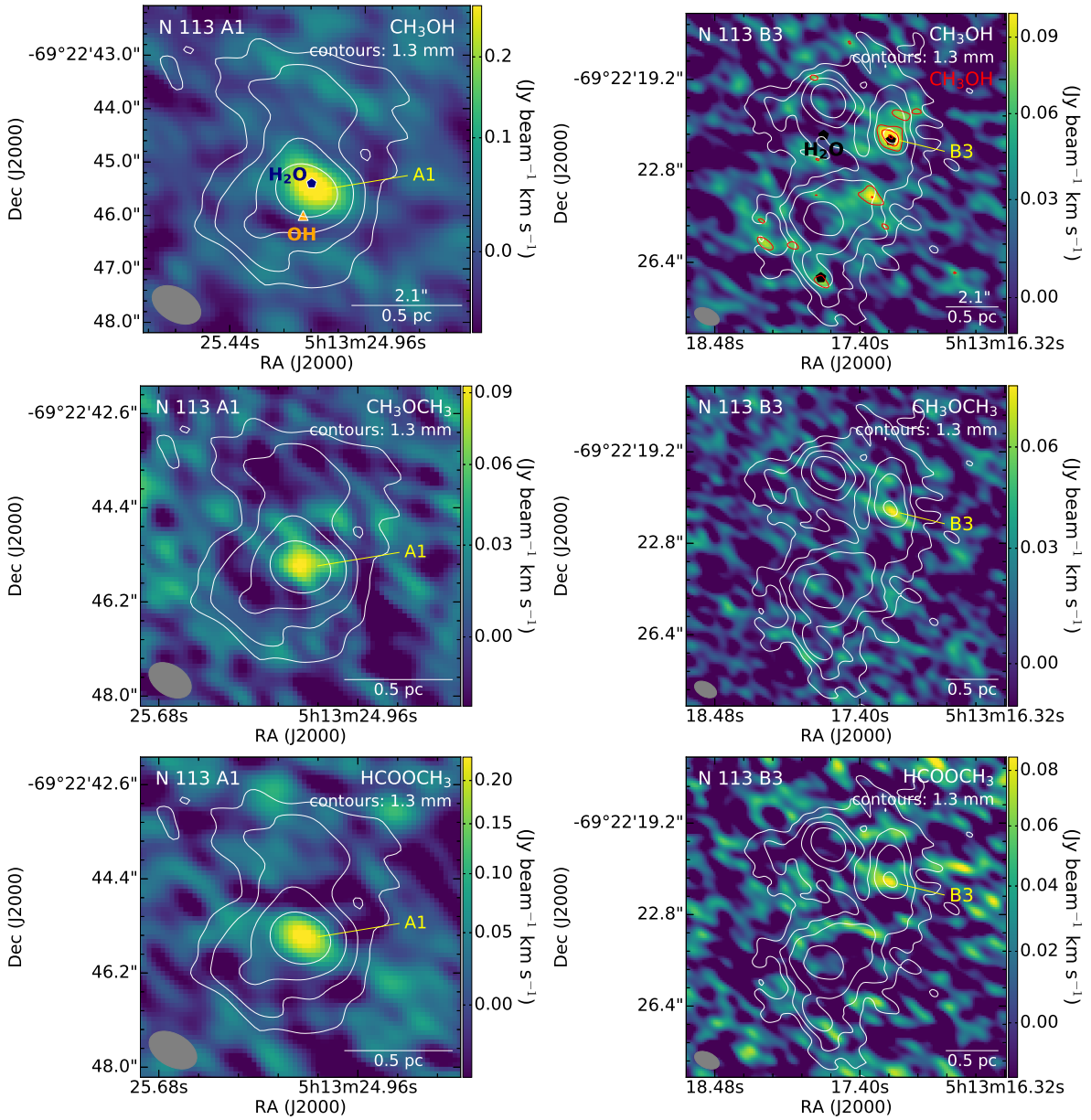

Figure 10: Integrated intensity images for CH_3OH (*top panel*; made using the channels corresponding to all CH_3OH transitions in the 216.9 GHz spectral window; see Table 5), CH_3OCH_3 (*middle panel*; the $13_{0,13}$–$12_{1,12}$ transition); and $HCOOCH_3$ (*bottom panel*; integrated over all detected transitions) for the A1 (*left column*) and B3 (*right column*) hot cores in the N 113 star-forming region. The H_2O and OH masers are indicated. The white contours correspond to the 1.3 mm continuum emission; the contour levels are the same as in Fig. 9. The red contours in the top right panel correspond to the CH_3OH emission with contour levels of (3, 5, 7) × 21 mJy beam^{-1}, the rms noise level of the CH_3OH integrated intensity image. The image shows the CH_3OH detection in other spots in the region ('Region B' in[18]) where no other COMs are detected. The results presented in this figure were reported in.[18] The ALMA beam size is shown in the lower left corner in each image.

$HCOOCH_3$ fractional abundances for a set of Galactic hot cores. When scaled by a factor of 2.5 to account for the lower metallicity in the LMC (the ratio between the solar metallicity and the metallicity of the LMC, assuming $Z_{\rm LMC} = 0.4\ Z_\odot$), the abundances of COMs detected in N 113 are comparable to those found at the lower end of the range in Galactic hot cores. This was a surprising result because previous observational and theoretical studies indicated that the abundance of CH_3OH in the LMC is very low.[18] concluded that COMs observed in the N113 hot cores could either originate from grain surface chemistry or in post-desorption gas chemistry.

The quartet $J = 2_K - 1_K$ of CH_3OH at ∼96.7 GHz was later detected serendipitously toward N 113 with ALMA in the project targeting two transitions (1–0 and 2–1) of three CO isotopes (^{12}CO, ^{13}CO, and $C^{18}O$) toward three LMC and three SMC star-forming regions with a resolution of ∼2″ (or ∼0.48 pc). N 113 is the only region in this sample with CH_3OH detection. The spectral window with the CH_3OH line was dedicated to the continuum observations and has a spectral resolution of ∼50 km s^{-1}. Such low spectral resolution does not allow for any quantitative analysis, but surprisingly the data revealed several additional well-defined CH_3OH peaks and extended emission in Region B (see Fig. 11). The CH_3OH emission reported in[18] was limited to two compact sources (hot cores A1 and B3) with some fainter emission detected in other locations in Region B (see Fig. 10); however, it was unclear whether the latter traces physically distinct sources or shocked lobes of the outflows.

In addition to hot cores, the ∼96.7 GHz CH_3OH emission is detected toward continuum sources B4, B7, and B6 in Region B and D1–D4 located toward the south (Fig. 11; Sewiło et al., in prep.). In Region A, the ∼96.7 GHz CH_3OH emission peak coincides with hot core A1; however, the emission extends toward the south.

The ∼96.7 GHz CH_3OH emission peaks in Regions A and B overlap with the SiO (5–4) peaks (with some faint extended emission visible throughout Region B, see Fig. 12;[18], Sewiło et al., in prep.), tracing shocks. The same regions are associated with the DCN (3–2) emission indicating their youth and are distributed along the dense gas filament. The

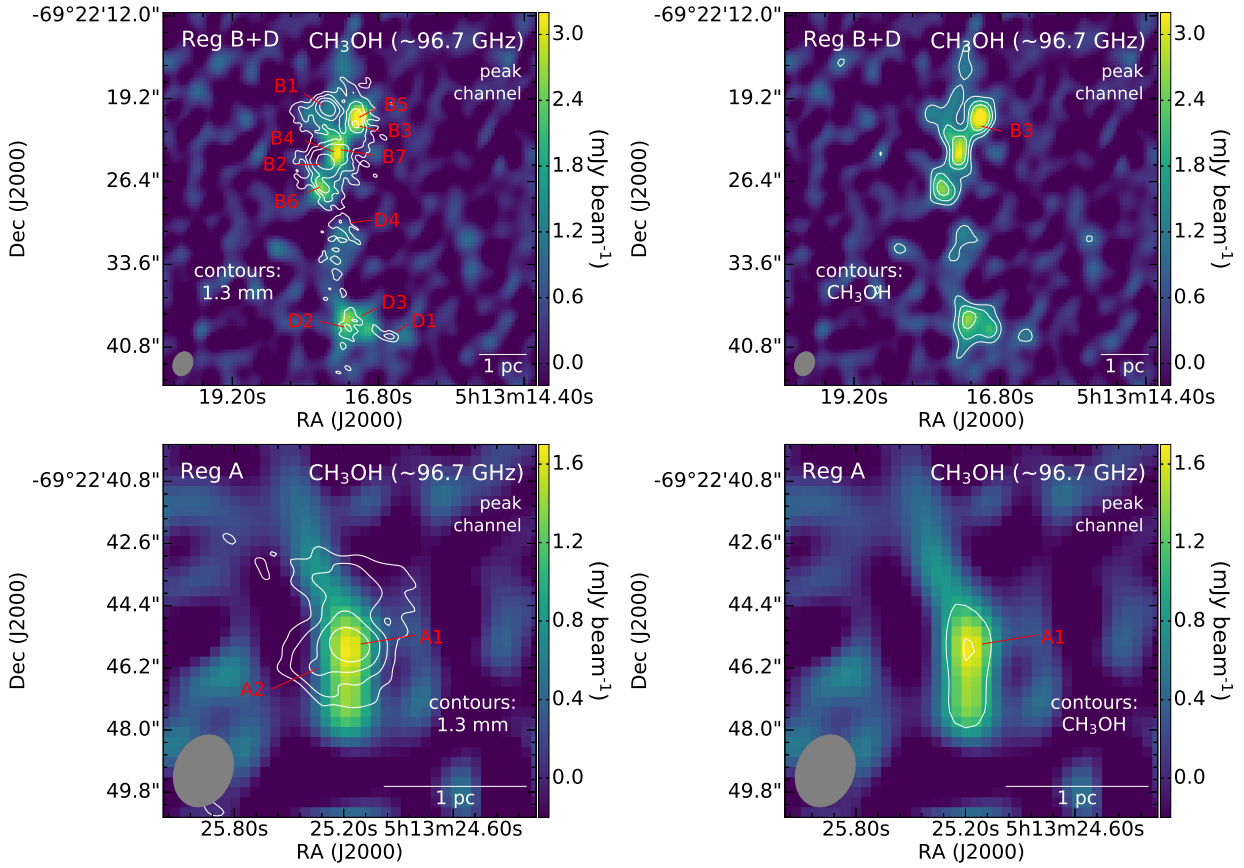

Figure 11: The single channel maps corresponding to the peak of the unresolved rotational transition quartet $J = 2_K - 1_K$ of CH_3OH at 96.7 GHz for regions in N 113 around and south of B3 (*top*) and toward A1 (*bottom*) hot cores (Sewiło et al., in prep.; ALMA 12m–Array data). The white 1.3 mm continuum contours in the left panel are the same as in Fig. 9. The white CH_3OH contours in the right panel correspond to (3, 5, 7) × rms noise level of the CH_3OH single-channel map of 0.32 mJy beam^{-1}. The ALMA beam size (2.″15 × 1.″66) for the CH_3OH observations is shown in the lower left corner in all images.

observational and theoretical studies indicate that the abundance of all deuterated species strongly depends on temperature: it drops rapidly with increasing gas temperature as an object evolves (see, e.g.,[88–91]) .

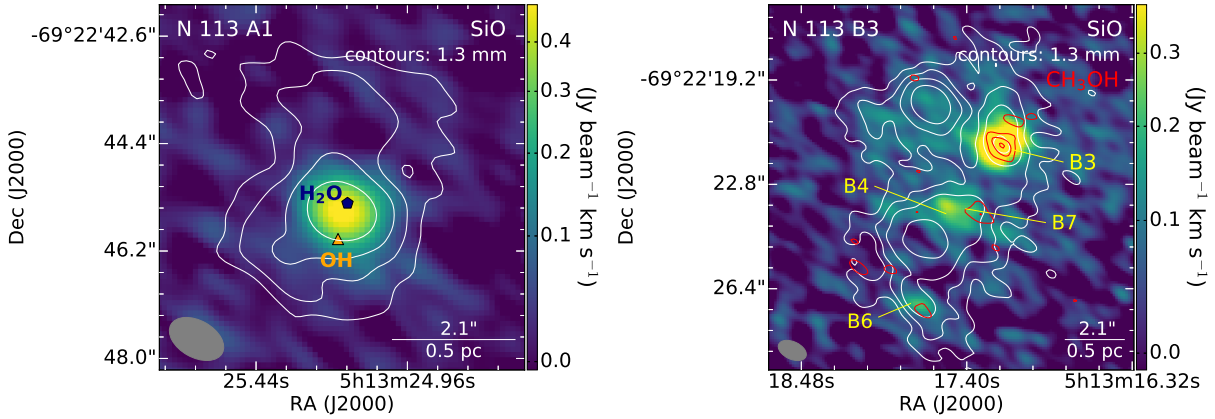

Figure 12: The SiO (5–4) integrated intensity images of N 113 A1 (*left*) and B3 (*right*) hot cores (Sewiło et al., in prep.). The contours are the same as in Fig. 9 (1.3 mm; *white*) and Fig. 10 (CH_3OH; *red*). The positions of H_2O and OH masers, and 1.3 mm continuum sources associated with the CH_3OH emission are indicated. The ALMA beam size ($0\farcs98 \times 0\farcs61$) is shown in the lower left corner in both images.

5 Theory

We can gain some insight as to the origin of the COMs detected in the Magellanic Clouds by comparing observations with current astrochemical theories of Galactic COM production in star-forming regions. Here we briefly review COM formation mechanisms and how they have been applied to low-metallicity environments.

5.1 Complex Molecule Formation in Star-forming Regions of the Milky Way

In the Galaxy, the largest COMs have until now been found primarily in the hot molecular cores associated with massive protostars, as well as with the so-called hot corinos found in regions of low-mass star formation (e.g.,[95]). In cold, dense molecular clouds some of these

Table 3: Chemical Abundances Relative to H_2 for COMs Detected in the LMC/SMC for Selected Galactic Hot Cores

Source	$N(X)/N(H_2)$			
	CH_3OH	$HCOOCH_3$	CH_3OCH_3	Ref.[a]
Orion Mol. Cloud:				
Hot core	1.4×10^{-7}	1.4×10^{-8}	8.0×10^{-9}	1
Compact Ridge	4.0×10^{-7}	3.0×10^{-8}	1.9×10^{-8}	1
G34.26−0.15:				
NE	8.5×10^{-7}	7.3×10^{-8}	1.4×10^{-7}	1
SE	6.4×10^{-7}	6.8×10^{-8}	8.5×10^{-8}	1
Sgr B2N	2.0×10^{-7}	1.0×10^{-9}	3.0×10^{-9}	1
G327.3−0.6	2.0×10^{-5}	2.0×10^{-6}	3.4×10^{-7}	1
AFGL 2591	7.0×10^{-7}	$<3.2 \times 10^{-7}$	$<1.0 \times 10^{-7}$	2
G24.78+0.08	6.5×10^{-7}	7.3×10^{-8}	3.0×10^{-7}	2
G75.78+0.34	9.2×10^{-7}	5.9×10^{-8}	1.9×10^{-7}	2
NGC 6334 IRS 1	4.0×10^{-6}	4.6×10^{-7}	2.4×10^{-6}	2
NGC 7538 IRS 1	5.7×10^{-7}	6.7×10^{-8}	$<7.6 \times 10^{-8}$	2
W3(H_2O)	5.4×10^{-6}	2.9×10^{-7}	8.3×10^{-7}	2
W33A	7.3×10^{-7}	9.6×10^{-8}	1.0×10^{-7}	2

[a] References: (1)[92] and references therein; (2).[93] For more information on Galactic hot cores, see also, e.g.,[94–96] and references therein.

organics have been known to be present for quite some time: HNCO, HCOOH, CH_2CO, CH_3CHO, CH_3OH (Ohishi & Kaifu 1992). More recently, the larger 'hot core' COMs, including CH_3OCH_3 and $HCOOCH_3$, have also been detected in several cold clouds ([97–101]). These detections have raised several challenges for existing theories of COM formation. These include the long-standing problem of identifying the mechanism responsible for returning ice-mantle molecules to the gas in cold clouds, and the fact that radical reactions on 10 K grains will not occur. In the case of the cold methanol detected in the LMC, it would appear that reactive desorption (i.e., using part of the energy released upon formation) is a plausible explanation.[102,103]

Hot cores are regions of high gas density and extinction where elevated dust temperatures have led to the sublimation of molecular ice mantles that have previously grown on cold dust grains. The first model of hot core chemical evolution was that of .[104] This involves a long period of cold (∼10 K) chemistry during which molecules form by gas–phase reactions and on dust grains, as the gas freezes out; this chemistry is similar to that found in cold dark clouds (e.g.,[105]). At some point gravitational collapse ensues, a protostar is formed, and the resulting large increase in luminosity heats the surrounding envelope of gas and dust to temperatures above about 100 K, leading to the sublimation of ice mantles and the formation of the hot core/corino. Further refinements to this picture have been (a) the addition of a slow 'warm-up' phase that can allow UV photolysis and radical–radical reactions to occur in the ice mantles, prior to formation of the hot core proper ([106]), and (b) gas–phase synthesis in the hot core, driven by the sublimated molecules ([107]). Further refinements have included the spatio-temporal evolution of the gas–grain chemistry ([108,109]).

Thus, within this simple picture, the complex molecules observed in hot cores can have four chemical origins: (1) formation in cold gas followed by freeze out on dust; (2) formation on the surfaces of cold (10 K) dust grains; (3) formation in UV-photolyzed ice mantles at ∼30 K; (4) *in situ* formation in hot core gas following ice sublimation.

5.1.1 Cold Gas–Phase Reactions in Dark Clouds

Cosmic-ray ionization of molecular hydrogen drives dense cloud chemistry by initiating sequences of ion-neutral and neutral–neutral reactions. This chemistry leads to the production of CO and many of the simple molecules detected in dark interstellar clouds. The complex molecules produced tend to be long hydrocarbon chains and associated radicals, such as the cyanopolyynes and various carbenes. The dark cloud TMC-1 in Taurus is recognized as the best example of this chemistry (e.g.,[110]) and chemical modeling demonstrates that gas-phase chemistry can account quite well for its composition (e.g.,[111]). It is now appreciated that methanol is formed entirely on dust grains (see Section 5.1.2) and so some (non-thermal) desorption mechanism is required to explain its presence in dark clouds like TMC-1 since dust temperatures are never sufficiently high for methanol and water to desorb. However, in dense cores where low-mass protostars are forming, it appears that some dust heating (to ∼30–35 K) has occurred and this can lead to the sublimation of more volatile molecules. In this Warm Carbon Chain Chemistry (WCCC), sublimation of large abundances of methane from the ice mantles greatly increases the efficiency of carbon-chain growth.[112] Although we do not discuss CH_4 injection further, the similarly warm dust temperatures found in the Magellanic Clouds may make this a viable route to widespread carbon chain formation there.

5.1.2 Cold Grain–Surface Reactions

Ice mantles grow on cold dust grains through the sticking of atoms of O, C and N followed by reactions with H atoms to form H_2O, CH_4 and NH_3. Molecules formed in the gas, such as CO and N_2, can also accrete and become incorporated in the mantle. Unsaturated molecules can undergo (tunneling) addition reactions with hydrogen atoms to produce molecular radicals that can further react and form new molecules (e.g.,[113]). Figure 13 shows that, in the case of CO, these processes can lead to a rich organic chemistry (e.g.,[114]) through the growth of linear chains by single atom additions and their subsequent saturation. This surface scheme can explain the presence of CH_3OH and many of the COMs known in hot

cores and originally made predictions[115] for new surface molecules (not shown) that were subsequently detected: glycolaldehyde[116,117], ethylene glycol ($(CH_2OH)_2$,[118]), acrolein and propionaldehyde.[119] Numerous surface chemistry experiments have validated many of these addition processes.[120–122]

5.1.3 COM Chemistry Driven by Sublimated Ice Mantles

[107] demonstrated that differences in mantle composition could, following sublimation , account for the chemical differentiation seen in the Orion–KL star-forming region. Rather than calculate the mantle composition *ab initio*, they assumed a composition based on observations and showed that the relative presence, or not, of methanol and ammonia could drive different chemistries in the hot gas (see also[123];[124]).[125] first suggested that self-methylation of methanol could be the source of dimethyl ether in hot cores, although they attributed its origin to be protostellar outflows rather than grain-surface chemistry. The self-methylation reaction is

$$CH_3OH_2^+ + CH_3OH \rightarrow CH_3OCH_4^+ + H_2O \quad (1)$$

where the neutral CH_3OCH_3 molecule is produced in reactions with either an electron or a base, such as ammonia. Based on laboratory experiments,[126] showed that, apart from CH_3OCH_3, many more large ethers and esters could be formed in this manner, in reactions involving ethanol, propanol and butanol.[127] Figure 13 includes alkylation reactions between protonated methanol and ethanol, the neutral alcohols, and formic acid. Methyl formate formation by methylation of HCOOH has also been studied in the laboratory[128] and shown to be a viable mechanism. In these experiments, the *trans*–HCOOH conformer of formic acid produced the protonated form of *trans*–$HCOOCH_3$; electron dissociative recombination, or proton transfer (see below), would then lead to the neutral ester. However, apart from one detection of *trans*–$HCOOCH_3$[129], it is the more stable *cis*–$HCOOCH_3$ conformer that is found in hot cores. It has therefore been suggested that interconversion between *trans*–$HCOOCH_3$ and *cis*–$HCOOCH_3$ structures could occur in the proton loss process.[130] Chemical

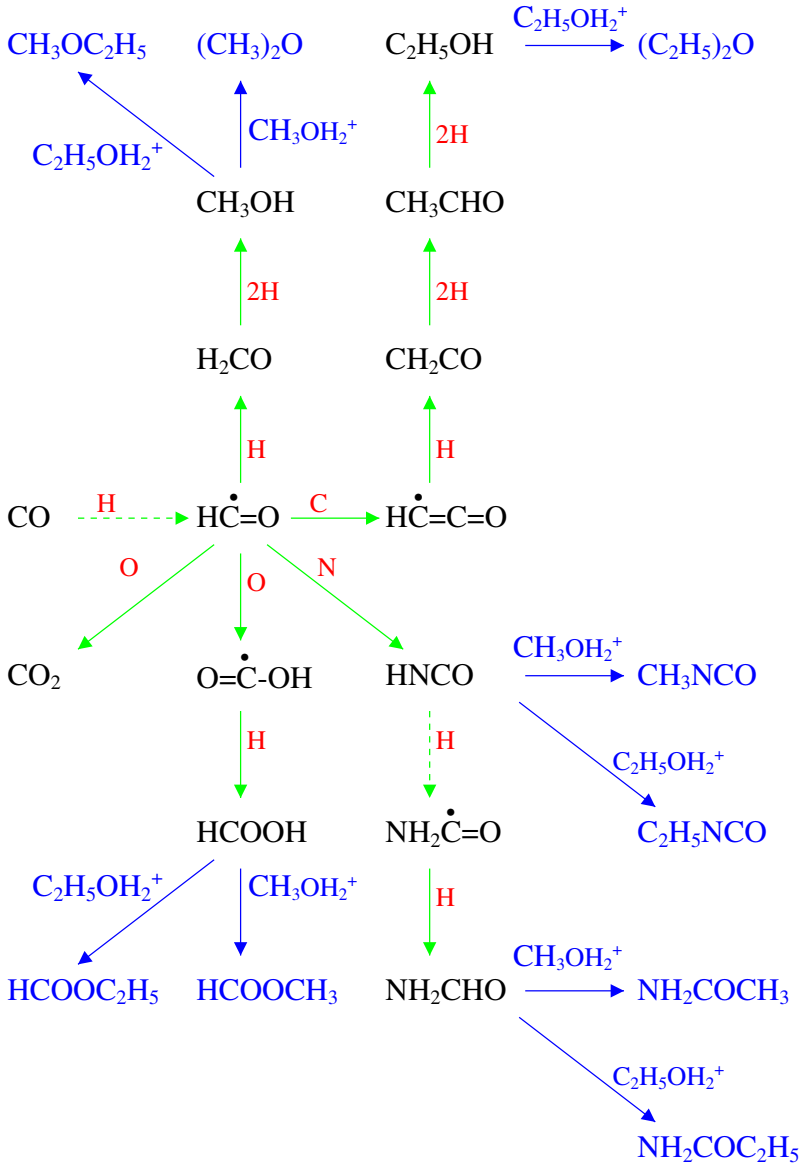

Figure 13: Interstellar gas–grain surface chemistry. Molecules involved in surface reactions are in black. Hydrogen atom addition to unsaturated molecules creates reactive radicals and additions of C, O and N atoms, allows a rich organic chemistry seeded by carbon monoxide to develop. Broken arrows indicate reactions with activation energy barriers; where 2H is shown, a barrier penetration reaction followed by an exothermic addition is implicitly indicated. Once these ice mantles have been sublimated into the hot core gas, methanol and ethanol can become protonated and take part in ion–molecule alkyl cation transfer reactions with themselves and with other molecules that were formed in the ices. These processes are denoted in blue and each arrow indicates the initial ion–molecule reaction and the production of the neutral COM, either through electron dissociative recombination or proton transfer to ammonia (adapted from[114] and references therein).

models have demonstrated that this is a very competitive pathway to $HCOOCH_3$ around protostars[131], assuming that interconversion proceeds with high efficiency.[132] Of the COM products shown in Fig. 13, apart from dimethyl ether and methyl formate, both ethyl formate and ethyl methyl ether have now been detected.[133,134]

A problem with this scenario has been that experiments on electron dissociative recombination of protonated COMs show that recovery of the neutral molecule occurs with a probability much lower than previously assumed, typically $< 5\%$ as compared to 100% (e.g.,[135]), and subsequently to COM abundances much lower than observed. However, if NH_3 is injected from grain mantles at moderate abundances, comparable with those measured in Galactic ices[136], then proton transfer, e.g.

$$CH_3OH_2^+ + NH_3 \rightarrow CH_3OCH_3 + NH_4^+ \tag{2}$$

can dominate COM formation and mitigate against the destructive effects of electron recombinations.[131,137]

As also shown in Fig. 13, gas phase COM formation driven by alkyl cation transfer reactions involving surface-formed HNCO and NH_2CHO could plausibly be a source of new molecules, perhaps explaining the hot core detections of methyl isocyanide (CH_3NCO) and acetamide (NH_2COCH_3).[138,139] However, the associated gas phase reactions have not yet been studied experimentally or theoretically and so should be regarded as speculative.

5.1.4 Radical Reactions in Icy Grain Mantles

As well as chemical reactions on grain surfaces driven by accretion of reactive species, it is also known that the ices can undergo bulk processing due to radiation damage caused by photons and energetic particles. Cosmic rays interact directly with icy mantles and recently chemical models have been developed to explore their effects on COM formation (see[140] and references therein). The environment of young protostars receives large doses of UV and

EUV radiation.[141] Even in dark clouds, a weak ambient flux of internal UV photons will exist[142] as energetic electrons produced by cosmic-ray ionization of molecular hydrogen can subsequently collide with, and excite, other H_2 molecules which undergo de-excitation by emission of Lyman and Werner band photons. The resulting UV flux is $\sim 10^3$ photons s^{-1} cm^{-2} which can be significant for chemistry in dense clouds. Laboratory experiments on UV photolysis of interstellar ice analogs show that an extensive organic chemistry can occur, primarily through reactions involving various radials produced from the major (parent) ice species (e.g.[143]) . Cold H additions to CO (see Section 5.1.2) have also to be considered since interstellar organic synthesis by photolysis requires that the methanol be present *ab initio* .[143,144]

Early theoretical models for organic synthesis from the recombination of radicals on cold grains appealed to physically unrealistic processes to attain the high mobilities needed for heavy particle migration and reaction.[145–149] Detailed modeling has shown that sustained UV photolysis and warming during the early stages of hot core evolution can produce many new organics.[106] In this picture, the ices are subjected to the Prasad–Tarafdar UV photons during the initial cold phase of core formation, producing a population of radicals. This irradiation can continue as the core is being gradually (as opposed to instantaneously) heated – the so called 'warm-up' phase.[106,150] When the dust grain temperature reaches, and can be maintained close to, about 30 K, the associated increase in radical mobility allows them to migrate and react. Radical–radical recombinations between HCO, CH_3O, CH_2OH, COOH and other simple radicals (e.g., CH_3, CH_2, NH_2, CN, OH) then produce many of the COMs observed in hot cores.[133,151,152]

5.2 Models of COM Formation in the Magellanic Clouds

Here we summarise and discuss theoretical models of COM formation at reduced metallicity in the light of recent observations.

5.2.1 Chemical Models of the LMC and SMC

[153] considered the chemical evolution of putative dark clouds in the LMC and SMC at the appropriate elemental depletions. They considered the purely gas-phase chemistry of fairly simple molecules, with only CH_3OH and CH_2CO being the only COMs. These models could produce CH_3OH abundances of $\sim 10^{-8}$; however, the main formation mechanism was through a radiative association process that is no longer considered viable.

More recently,[154,155] developed gas–grain models of the LMC and SMC. Again, cold dark clouds were modeled for a wider range of physical parameters, including appropriately warmer gas and dust temperatures. In these models CH_3OH was formed by CO hydrogenation on dust grains. For the LMC, they found that molecular abundances similar to Milky Way dark clouds could be obtained, whereas for the SMC the abundances were lower for most molecules. The model predictions were compared to several star-forming regions in the LMC (as no data on Magellanic dark clouds then existed): N 159W, N 159S, N 160, and 30 Dor–10. When compared to the Magellanic source N 159W with a thermal methanol detection, the calculated abundances were found to be $\sim$10–10^3 times lower than determined by.[16] The reason for this discrepancy was explained as being due to the warm dust temperatures, appropriate for Magellanic dark clouds, that were considered in the models. Dust temperature affects grain-surface chemistry and can inhibit methanol formation since, for temperatures above about 15 K, hydrogen atoms will desorb before they can react with CO. Above about 25 K, CO molecules residing in CO-rich outer layers of the ice mantle will also sublimate , whereas those trapped in the H_2O ice matrix require higher dust temperatures.[156] In both the LMC and SMC gaseous NH_3 abundances of $\sim 10^{-8}$ were found. For models with dust temperatures more similar to the Milky Way ($\sim$10–15 K), the dust ice mantles are predicted to contain large fractions of CH_3OH ($\sim$10–40%) and NH_3 ($\sim$1–7%). Hence, the presence of CH_3OH in the Magellanic Clouds points to formation in a cold pre-hot core phase.

[157] studied the formation of ice mantles in the Magellanic Clouds but instead employed a correct stochastic calculation of the grain chemistry. The relative composition of ices

comprising of H_2O, CO, CO_2, CH_3OH, NH_3 and CH_4 were calculated as a function of the interstellar UV radiation field. The CH_3OH and NH_3 ice fractions were found to be lower ($\sim$ few%) than those found by[154,155] and more compatible with those of Galactic ices.[136]

[158] reported the first *bona fide* hot core models of the Magellanic Clouds. Their model was a standard three-phase model (cold quasistatic phase, collapse phase with out without 'warm-up', and hot core phase; see Section 5.1) and included the radical chemistry induced during the 'warm-up' phase as well as many of the COMs known in Galactic hot cores ([106,151]; see Section 5.1.4). When compared to the N 113 observations, only one of the models (a 100 K core in which the initial phase of core formation proceeded at 10 K, Model 1) reproduced the observed CH_3OH abundances in both A1 and B3 at times (post- sublimation) when CH_3OCH_3 and $HCOOCH_3$ had non-trivial abundances. As CH_3OH is the proposed parent of CH_3OCH_3 and $HCOOCH_3$ in both grain-surface reactions (see Section 5.1.4) and in ion–molecule reactions (see Fig. 13) the comparison of predicted CH_3OCH_3/CH_3OH and $HCOOCH_3/CH_3OH$ ratios with observations provides the most stringent tests of their origin (see Section 5.2.2). The relevant[158] model yields $HCOOCH_3/CH_3OH$ ratios of $\sim$0.04 in good agreement with that of both N 113 cores; whereas the CH_3OCH_3/CH_3OH ratios are about 5 times greater than observed.

Overall, these models indicate that the hot cores in the Magellanic Clouds must have undergone a period of chemical evolution when the dust was cold, as in theories of Galactic hot core formation.

5.2.2 Models for COM Ice–Gas Synthesis

Given the importance of NH_3 for gaseous COM formation, the Magellanic Clouds offer a potential opportunity to test this scenario in a low-metallicity environment.[158] emphasized the sublimation of COM-containing ice mantles into the hot gas, not active formation *in situ*, as the possible source of Magellanic COMs. Post-sublimation gas-phase synthesis (see Section 5.1.3) has not yet been studied in the context of the Magellanic Clouds and here we

report relevant model calculations as a first approximation.

Table 4: Model Ice Mantle Compositions[a]

Molecule	LMC	SMC
H_2O	4.5×10^{-5}	2.2×10^{-5}
CO	1.7×10^{-5}	7.6×10^{-6}
CO_2	1.3×10^{-5}	6.0×10^{-6}
CH_4	2.1×10^{-6}	1.0×10^{-6}
NH_3	1.0×10^{-6}	3.2×10^{-7}
N_2	3.2×10^{-6}	1.0×10^{-6}
H_2CO	1.1×10^{-6}	5.0×10^{-7}
CH_3OH	3.2×10^{-6}	1.4×10^{-6}
HCOOH	6.4×10^{-7}	3.2×10^{-7}

[a] Abundances are given relative to total density of hydrogen nuclei.

The calculations were performed with the dynamical-chemical model of[131] but modified according to the simplest version of these models in which the physical conditions are fixed in time and the ices are injected instantaneously into the hot gas at $t = 0$ (cf.[107]), as opposed to computing the physical and chemical evolution of the core (e.g., gravitational collapse, protostellar luminosity heating, time-dependent molecule desorption). Table 4 lists the assumed ice mantle compositions. These were obtained by scaling the ice abundances from Table 1 of[131] to the elemental depletions observed in the SMC and LMC clouds as listed in Table 1 of[154] ($f_{\mathrm{LMC},i}$) and[155] ($f_{\mathrm{SMC},i}$), respectively. The (C, O, N) scaling factors ($1/f$) are (0.41, 0.46, 0.21) for the LMC and (0.20, 0.22, 0.064) for the SMC; for each molecule listed in Table 4, we used the averaged $1/f$ of its corresponding elements to determine initial ice abundances in the LMC/SMC from their Galactic values used by.[131] Typical hot core physical conditions were assumed: $n_{\mathrm{H_2}} = 5{\times}10^7$ cm^{-3}, T=150 K, and a cosmic-ray ionization rate $\zeta = 3 \times 10^{-17}$ s^{-1}. The chemical network is as discussed in.[131] Figure 14 shows COM chemical evolution in hot core models applicable to the LMC and SMC. Generally, one can notice a decrease of all gas phase abundances by a factor of a few depending on the elemental depletion of C, N, and O in the two galaxies. However, the stronger N depletion relative to C and O (by a factor of 2 and 4 for the LMC and SMC, respectively) induces a more pronounced decrease of NH_3 relative to other ice species.

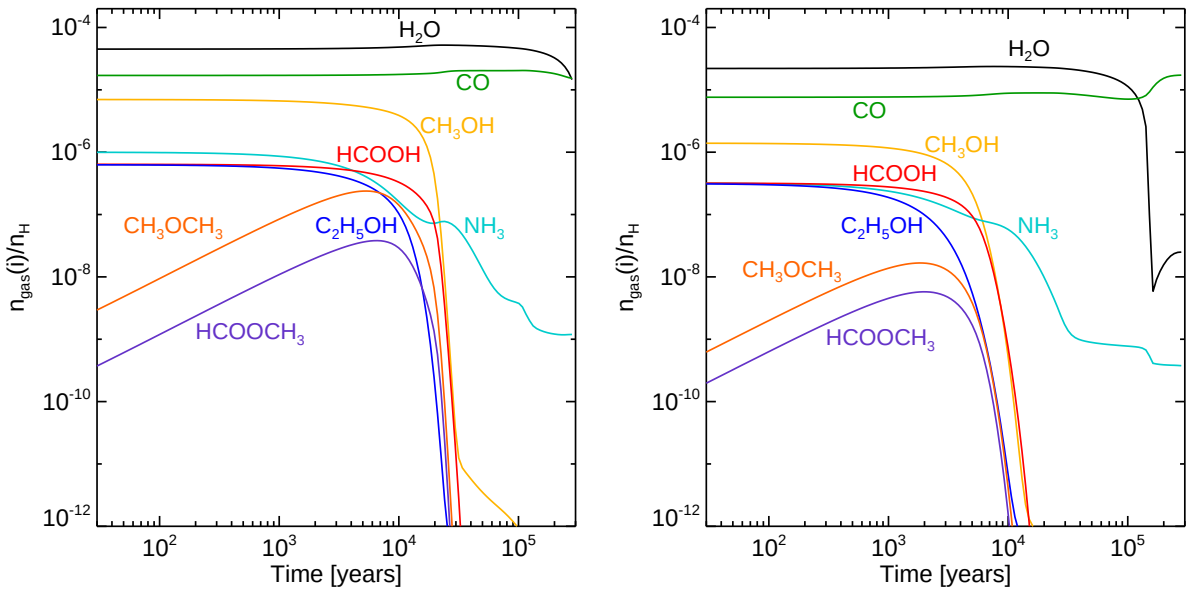

Figure 14: Chemical evolution in hot core models of the LMC (*left panel*) and SMC (*right panel*). Ice mantles with the compositions of Table 4 are instantaneously injected into the gas at $t = 0$.

As found by[131], a decrease of the injected ice mantle NH_3/CH_3OH abundance ratio from $\sim$1 decreases the production efficiency of complex organic molecules; for CH_3OCH_3 and $HCOOCH_3$ the Magellanic Cloud abundances are lower by a factor of 3 for the LMC and of 5 for the SMC. The NH_3 abundance is not observationally well-constrained in the LMC and SMC and is unknown in the N 113 region. In the LMC,[36] measured an ammonia abundance of $\sim 4\times10^{-10}$ in N 159W and Fig. 15 shows that systematically reducing the injected NH_3 abundance from ices dramatically lowers the COM abundances. However, any decline in COMs below an NH_3 abundance of $\sim 10^{-8}$, down to the level measured by[36], is halted as electron dissociative recombinations come to dominate the loss of molecular ions. Although models of ice formation in the Magellanic Clouds do predict NH_3/H_2O mantle fractions sufficiently large to allow efficient ion–molecule formation in the LMC (see Section 5.2.1), NH_3 observations of N113 and other COM-containing regions are clearly required to validate the efficacy of this process.

The observed abundances of CH_3OCH_3 and $HCOOCH_3$ in the A1 and B3 hot cores of

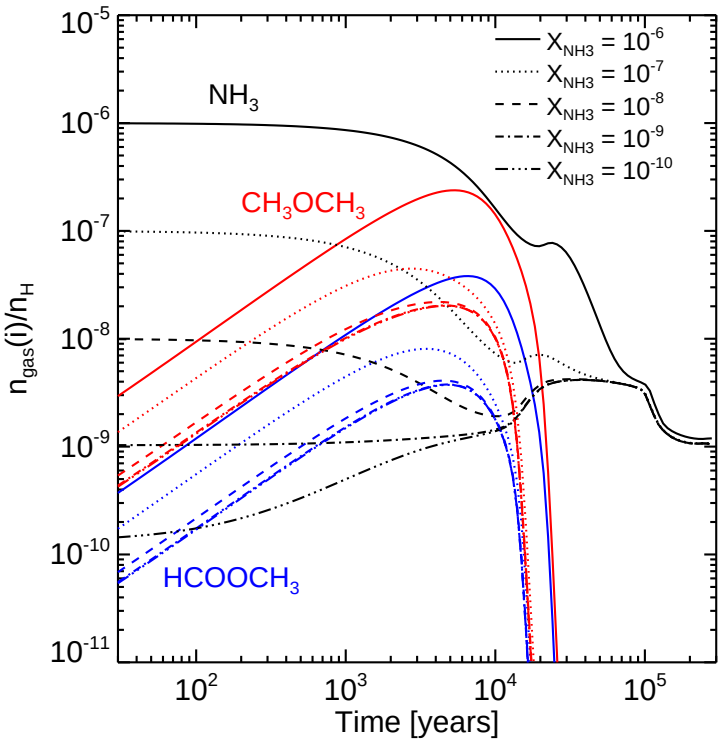

Figure 15: Evolution of CH_3OCH_3 and $HCOOCH_3$ abundances in the LMC model as a function of the NH_3 abundance sublimated from ices.

N 113 (see Table 3) can be reproduced in the models of Fig. 14 despite the lower elemental depletions. However, as in the case of Galactic hot core models these do not occur at a time when the CH_3OCH_3/CH_3OH and $HCOOCH_3/CH_3OH$ abundance ratios have their observed values (Fig. 16). In the LMC, when the methanol abundance is $\sim 10^{-8}$, the observed CH_3OCH_3/CH_3OH ratios in A1 ($\sim$0.1) and B3 ($\sim$0.2) are about an order of magnitude higher than the calculated values ($\sim$0.01); for $HCOOCH_3/CH_3OH$ the calculated value of ($\sim$0.003) is about a factor 20 too low.

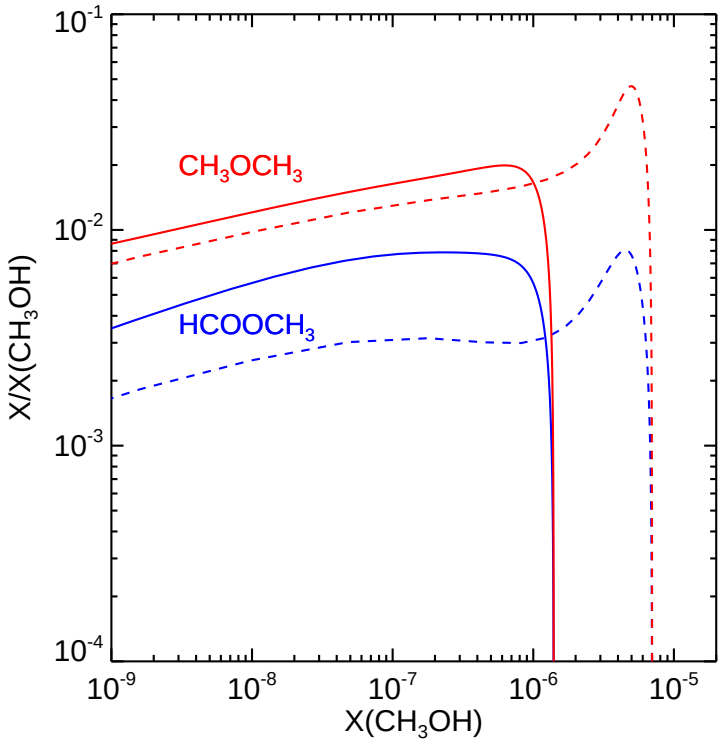

Figure 16: Evolution of the CH_3OCH_3/CH_3OH and $HCOOCH_3/CH_3OH$ abundance ratios in the models of Fig. 14 for the LMC (solid curves) and SMC (dashed curves).

[158] claimed a very good agreement with the abundances of[18] to within a factor of 5. However, calculated abundances and the observed abundances were presented as relative to total hydrogen density and molecular hydrogen density, respectively. Correcting the abundance comparison by the factor of 2 means that for CH_3OCH_3 in A1 and B3, the models overpredict the abundances by factors of 12–20; only the calculated abundances of

CH_3OH and $HCOOCH_3$ in A1 agree to within a factor of 5.

When a detailed treatment of the collapse physics is included in hot core chemistry models, a monotonic increase in the radial gas and dust temperatures occurs as a function of the increasing (accretion) luminosity of the protostar (e.g.,[108]). In the case of Galactic hot cores/corinos,[131] showed that molecular *recondensation* may be just as chemically important as molecular depletion onto dust in cold cores, and sublimation from them in hot cores. This can occur if the accretion onto the protostar is not monotonic but sporadic.[159] Once grains have been raised to a temperature of about 120 K or more, most of the ice mantle is removed and, as they cool to 50 K or lower in about 100 years, selective recondensation can occur due to the differing binding energies for physisorption. Production of organic molecules ensues in the brief post- sublimation period, as in the standard model, except that the products subsequently condense as ices.[131] demonstrated that the observed large CH_3OCH_3/CH_3OH and $HCOOCH_3/CH_3OH$ ratios could be reproduced due to the relatively higher binding energy of CH_3OH. This may be a fundamental process for the organic chemistry of material near protostars as, between sublimation–recondensation events, there can be a mantle-driven gaseous chemistry leading to the dust grains being coated with the products as they cool. This scenario remains to be evaluated in the context of Magellanic Cloud hot cores.

6 Discussion

Although single-dish observations provided the first detections of methanol in two bright regions in the LMC (N 159 and N 113), it was ALMA with its unprecedented angular resolution and sensitivity that has started and continue revolutionizing the field of complex organic chemistry in low-metallicity environments. To date, the sample of sources with COMs detection is very small and diverse. Only two *bona fide* hot cores with COMs are known in the Magellanic Clouds, both in the N 113 star-forming region in the LMC (N 113 A1 and B3;[18]). Another hot core in the LMC (ST 11) was found by[73], but no methanol or other COMs were

detected. The detection of methanol was reported for two other sources, one in the LMC (N 159W–S, Section A.1) and one in the SMC (IRAS 01042−7215,[19]), but not in hot cores ('cold methanol'). Several sources in N 113 (in addition to two hot cores) are associated with methanol, but due to a very low spectral resolution of the observations, a determination of their physical parameters based on the existing data is currently impossible.

No firm conclusions about complex organic chemistry under reduced metallicity conditions can be drawn based on the current sample of sources with the detection of COMs. However, some general trends are noticeable.

None of the sources with a COMs detection is associated with an infrared source: COMs are detected toward mm continuum sources in the vicinity of bright *Spitzer* YSOs. ST 11 with no COMs detection but with evidence for hot core chemistry is the only source associated with the infrared source. In fact, this is the brightest *Spitzer* YSO in the entire N 144 H II region[51]; higher resolution near-infrared observations reveal a cluster with one dominating source (see Fig. 2), which likely has the largest contribution to the emission at longer wavelengths. Multiple mm continuum sources are detected toward all the other fields. The N 113 B3 field is particularly interesting since it harbors sources at different evolutionary stages including a hot core and ultra-compact H II regions with younger sources distributed along a dense gas filament (see Figs. 9 and 12). Several mm continuum sources including one associated with the brightest CH_3OH peaks in the region, are also found along the filament in N 159W–S (see Figs. 4–5 and[76]).

The detection of cold methanol in N 159W–S and IRAS 01042−7215 P2/P3 is puzzling, however, similar results are being obtained in our Galaxy. In Galactic dark clouds, gas–phase methanol is found to have a clumpy distribution, often not following the density distribution traced by continuum and molecular tracers[160], and thus provides evidence of rapid ice desorption processes. This methanol tends to be cold, at excitation temperatures of 5–20 K, similar to what is observed in N 159W–S and IRAS 01042−7215. In the Barnard 5 cloud in particular, a cold methanol clump with the CH_3OH abundance with respect to H_2 of

Table 5: COM Transitions Detected in the Magellanic Clouds with ALMA[a]

Species	Transition	Frequency (GHz)	E_U (K)	Detection[b]	
	LMC N 113			A1	B3
CH_3OH v_t=0	$5_{1,4}$–$4_{2,2}$ E	216.94560	55.87	+	+
CH_3OH v_t=1	$6_{1,5}$–$7_{2,6}$ A^-	217.299205	373.93	+	+
CH_3OH v_t=0	$20_{1,19}$-$20_{0,20}$ E	217.88639	508.38	+	−
CH_3OH v_t=0	$10_{2,9}$-$9_{3,6}$ A^-	231.28110	165.35	+	+
CH_3OH v_t=0	$10_{2,8}$-$9_{3,7}$ A^+	232.41859	165.40	+	+
CH_3OH v_t=0	$18_{3,16}$-$17_{4,13}$ A^+	232.78350	446.53	+	+
CH_3OH v_t=0[c]	$2_{-1,2}$–$1_{-1,1}$ E	96.739362	12.54	+	+
	$2_{0,2}$–$1_{0,1}$ A^+	96.741375	6.97		
	$2_{0,2}$–$1_{0,1}$ E	96.744550	20.09		
	$2_{1,1}$–$1_{1,0}$ E	96.755511	28.01		
$HCOOCH_3$ v=0	$18_{2,16}$–$17_{2,15}$ E	216.83020	105.68	+?	−
$HCOOCH_3$ v=0	$18_{2,16}$–$17_{2,15}$ A	216.83889	105.67	+?	−
$HCOOCH_3$ v=0	$20_{1,20}$–$19_{1,19}$ E	216.96476	111.50	+	+?
$HCOOCH_3$ v=0	$20_{1,20}$–$19_{1,19}$ A	216.96590	111.48	+	+?
$HCOOCH_3$ v=0	$20_{0,20}$–$19_{0,19}$ E	216.96625	111.50	+	+?
$HCOOCH_3$ v=0	$20_{0,20}$–$19_{0,19}$ A	216.96742	111.48	+	+?
CH_3OCH_3	$13_{0,13}$–$12_{1,12}$ EE	231.98782	80.92	+	+
	LMC N 159W–S			MMS–3[d]	
CH_3OH v_t=0	$5_{0,5}$–$4_{0,4}$ E	241.700219	47.93	+	
CH_3OH v_t=0	$5_{-1,5}$–$4_{-1,4}$ E	241.767224	40.39	+	
CH_3OH v_t=0	$5_{0,5}$–$4_{0,4}$ A^+	241.791431	34.82	+	
CH_3OH v_t=0	$5_{1,4}$–$4_{1,3}$ E	241.879073	55.87	+	
CH_3OH v_t=0[e]	$5_{-2,4}$–$4_{-2,3}$ E	241.904152	60.72	+	
	$5_{2,3}$–$4_{2,2}$ E	241.904645	57.07		
	SMC IRAS 01042−7215			P2	P3
CH_3OH v_t=0	$5_{0,5}$–$4_{0,4}$ A^+	241.791431	34.82	+	+
CH_3OH v_t=0	$5_{-1,5}$–$4_{-1,4}$ E	241.767224	40.39	+	+
CH_3OH v_t=0	$5_{0,5}$–$4_{0,4}$ E	241.700219	47.93	+?	−
CH_3OH v_t=0[e]	$5_{-2,4}$–$4_{-2,3}$ E	241.904152	60.72	+	−
	$5_{2,3}$–$4_{2,2}$ E	241.904645	57.07		

[a] The table uses the CDMS notation from the Splatalogue. See footnotes to Table 1 for details; [b] The symbols in these columns indicate a detection ('+'), a tentative detection ('+?'), or a non-detection ('−') of a given molecular line transition; [c] The four transitions at ∼96.7 GHz are blended; the spectral resolution of these observations which were dedicated to the continuum detection is ∼50 km s^{-1}. In addition to hot cores A1 and B3, there are several other ∼96.7 GHz CH_3OH peaks in N 113 (see Section 4.3); [d] The two methanol peaks associated with MMS–3 where the largest number of CH_3OH lines are detected and the temperature fitting is the most reliable (see Section 4.2.1); [e] The CH_3OH lines at 241.904152 GHz and 241.904645 GHz are blended.

$\sim 4 \times 10^{-8}$, offset from the IRAS sources, has proven to be a signpost of ice desorption – first by the detection of cold gas–phase water at abundances similar to methanol[161] and then other COMs like CH_3CHO and $HCOOCH_3$, likely formed by gas–phase chemistry following an event of ice desorption.[101] However, the low yield of COMs from ice desorption at cold temperatures is at most a few percent of methanol even at Galactic metallicities, thus consistent with non-detections of COMs towards N 159W–S, IRAS 01042−7215 P2 and P3.

For IRAS 01042−7215 where the CH_3OH emission is detected toward two sources corresponding to the continuum peak,[19] discussed three possibilities for the nature of P2/P3 (their 'East core') where cold methanol was detected – they suggested it can be either a massive starless core, an embedded high-mass YSO (or multiple YSOs) before the emergence of infrared emission, or a cluster of low-mass embedded YSOs.

Observations confirm that COMs can form in extragalactic environments. Formation pathways have been suggested that involve either grain–surface chemistry or gas–phase chemistry, or a combination of both. Theoretical models accounting for the physical conditions and metallicity of hot molecular cores in the Magellanic Clouds have been able to broadly account for the existing observations.

As cosmic metallicity is increasing with time, understanding interstellar chemistry in low metallicity environments also gives us insight into the chemistry of the past Universe. The detection of COMs in the Magellanic Clouds has important implications for astrobiology. The metallicity of the LMC/SMC is similar to the mean metallicity of the interstellar medium during the epoch of peak star formation in the Universe, thus the presence of COMs in these systems indicates that a similar prebiotic chemistry leading to the emergence of life, as it happened on Earth, is possible in low-metallicity systems in earlier epochs of the Universe. According to one of the theories on the emergence of life on Earth, interstellar COMs (after incorporating into comets) might have been delivered to early Earth to provide important ingredients for the origin of life (e.g.,[1,89,162]).

COMs more complex than CH_3OH are detected in the LMC toward hot cores which are

associated with massive stars and therefore are short-lived; a detection of COMs does not have a direct relation to the origin of life at these locations. However, if COMs are detected toward hot cores, we can expect them to be present in hot corinos, which are associated with low-mass stars. The evolution of low-mass stars is long enough for life to emerge if favorable conditions exist.

7 Future Prospects

Systematic studies on YSOs in different environments in the LMC and SMC are needed to build a statistically significant sample of sources with COMs detections in the Magellanic Clouds that would allow us to draw reliable conclusions on the formation and evolution of COMs in reduced metallicity environments. Both the LMC and SMC samples will be important to get as wide a range of metallicities as possible. In the SMC, the metallicity is lower than in the LMC (as low as 0.1 $Z_{\odot}$ in the SMC tail where star formation occurs in pockets; e.g.,[163]) and the formation and survival of COMs can be tested in an even harsher environment. Enlarging the sample in both galaxies is important to distinguishing between local environmental conditions in individual clouds, and the more global effect of metallicity.

Reliable determination of Magellanic Clouds hot cores' physical and chemical properties and a comparison between the two Clouds and the Galaxy are of paramount importance to understand the impact of metallicity on complex organic chemistry. High-resolution and sensitivity observations of known hot cores in the Magellanic Clouds as their number starts increasing are a natural next step in reaching this goal. This direction of research involves chemical modeling of hot cores to understand their chemical evolution.

ALMA programs are underway targeting tens of YSOs identified by *Spitzer* and *Herschel*, both specifically designed to search for COMs and those with different science goals, but covering frequency ranges where COMs can be detected (serendipitous detections as in N 113). ALMA's broad spectral windows allow to observe many spectral lines simultaneously with

the spectral setup covering the most important molecules.

What new COMs await discovery in the Magellanic Clouds? Chemical models of the LMC have not been successful (to within an order of magnitude) in accounting for the observed presence of dimethyl ether in the LMC (see Section 5.2.2) and so may not be reliable indicators for new molecules. At present, taking the inventory of well-studied Galactic hot cores may provide the best guidelines for future searches. Molecules that could be expected to present include acetaldehyde, ethanol, ethyl cyanide, isocyanic acid, and formamide.

The NASA's *James Webb Space Telescope* (*JWST*; scheduled to launch in 2021) near- (0.6–5.3μm; the Near Infrared Spectrograph – NIRSpec instrument) to mid-infrared (4.9–28.8 μm; Mid-Infrared Instrument – MIRI) observations will enable studies of the solid phase material in different Galactic and extragalactic environments. The high sensitivity and angular resolution of *JWST* will enable detailed studies of hot cores in the Magellanic Clouds on $\sim$0.04 pc scales in the near-infrared, without contamination from the surrounding regions. It will be possible to do an inventory of simple (e.g., H_2O, CO_2, CO) and complex (CH_3OH and beyond, including molecules of prebiotic significance) ices in the low-metallicity environments in the Magellanic Clouds. For example, in the 5–8 μm range (MIRI) COMs such as ethylene glycol, glycolaldehyde, methyl formate, and dimethyl ether (the latter two already detected in N 113 A1/B3 in the gas phase with ALMA), and others can be detected.[164] The laboratory experiments are underway predicting which COMs can be detected at shorter wavelengths covered by NIRSpec. Such studies will provide information on differences in chemical complexity of hot cores in different environments.

A Technical Details on Unpublished Observations Reported in this Paper

The ALMA and *VLT*/KMOS data presented in Section 4.2.1 for N 159W–S have not been published in literature yet. Below we summarize technical details of these observations.

A.1 ALMA

N159W–S was observed with ALMA (Atacama Large Millimeter/submillimeter Array; ALMA Partnership et al. 2015) during its Cycle 4 in October 2016 as part of project number 2016.1.00308.S. We used the main array (i.e.,12m antennas) consisting of 40 antennas. The phase center was set to RA (J2000) = $05^{h}39^{m}41^{s}$, Dec (J2000) = $69°46'11''$. The ALMA correlator was configured to cover specific frequency ranges within the Band 6 of ALMA. Four broad spectral windows (with a bandwidth of 1875 MHz each) centered at frequencies 242.4, 244.8, 257.85 and 259.7 GHz were tuned at the frequencies of specific molecular transitions of dense gas, shock/hot core tracers (e.g., CS, SO_2, CH_3OH and SiO). The ALMA data were calibrated using the ALMA calibration pipeline available in CASA version 5.5.1. Flux calibration was obtained through observations of the bright quasar J0519–4546. The gains were calibrated by interleaved observations of the quasar J0601–7036. The bandpass response was obtained by observing the bright quasar J0635–7516. After the calibration was applied, the line-free channels of the broad spectral windows were identified and used to create the continuum images. The CLEANing process was done with the task TCLEAN, and setting the robust parameter of Briggs equal to 0.5 as compromise between resolution and sensitivity. The resulting images were restored with a synthesized beam of $0\farcs22\times0\farcs12$. Sensitivity of 1.4 mJy beam^{-1} was achieved in the data cube covering the CH_3OH lines.

A.2 *VLT*/KMOS

N159W–S was observed with *VLT*/KMOS (*Very Large Telescope*/$K-$band Multi-Object Spectrograph) under program 0101.C-0856(A) using the $H + K$ grating with a spectral resolving power of 2000. The observations were carried out using a standard nod-to-sky procedure with an integration time of 150 s, four DITs and three dither positions, yielding a total on-source integration time of 1800 s. Telluric absorption correction, response curve correction, and absolute flux calibration was carried out using observations of telluric standard stars using three IFUs. The data were reduced with the standard *VLT*/KMOS pipeline

using the ESOREFLEX data reduction package. The $K-$band continuum image is produced by integrating over a third-order polynomial fit to the data for every spatial pixel (spaxel) over the spectral range 2.028–2.290 μm. The Brγ and H_2 line emission images are produced by fitting a Gaussian profile to the emission lines at every position in the image.

Acknowledgement

We thank Dr. Kazuki Tokuda for providing the ALMA 1.3 mm continuum image of N159W–S and Dr. Julia Roman-Duval for providing the CH_3OH ~96.7 GHz image of N 113. We also thank Dr. Gerard Testor for providing the *VLT*/NACO near-infrared images that were used to improve astrometry of the *VLT*/KMOS images. The work of M. S. was supported by NASA under award number 80GSFC17M0002. The work of S. B. C. was supported by the NASA Astrobiology Institute through the Goddard Center for Astrobiology. P. S. acknowledges support from the University of Cologne, Collaborative Research Centre 956, subproject C3, funded by the Deutsche Forschungsgemeinschaft (DFG) – project ID 18401886, and Verbundforschung Astrophysics, Project 05A17PK1, funded by BMBF (German Ministry of Science and Education). V. T. acknowledges the financial support from the European Union's Horizon 2020 research and innovation programme under the Marie Skłodowska-Curie grant agreement No. 664931. E. S. W. received funding from the Swedish National Space Agency, grants dnr 98/14 and dnr 246/16. The work of J. W. was supported by Sonderforschungsbereich SFB 881 "The Milky Way System" (subproject B2) of the German Research Foundation (DFG). The work of S. Z. and T. O. were supported by NAOJ ALMA Scientific Research Grant Number 2016-03B. The work of T. O. was also supported by JSPS KAKENHI (Grant Nos. 22244014, 26247026, and 18H05440). The work of A. K. was supported by JSPS KAKENHI (Grant No. 23403001). The authors acknowledge financial support from their home institutions.

References

(1) Ehrenfreund, P.; Charnley, S. B. Organic Molecules in the Interstellar Medium, Comets, and Meteorites: A Voyage from Dark Clouds to the Early Earth. *ARA&A* **2000**, *38*, 427–483.

(2) Pietrzyński, G. et al. An eclipsing-binary distance to the Large Magellanic Cloud accurate to two per cent. *Nature* **2013**, *495*, 76–79.

(3) Graczyk, D.; Pietrzyński, G.; Thompson, I. B.; Gieren, W.; Pilecki, B.; Konorski, P.; Udalski, A.; Soszyński, I.; Villanova, S.; Górski, M.; Suchomska, K.; Karczmarek, P.; Kudritzki, R.-P.; Bresolin, F.; Gallenne, A. The Araucaria Project. The Distance to the Small Magellanic Cloud from Late-type Eclipsing Binaries. *ApJ* **2014**, *780*, 59.

(4) Asplund, M.; Grevesse, N.; Sauval, A. J.; Scott, P. The Chemical Composition of the Sun. *ARA&A* **2009**, *47*, 481–522.

(5) Russell, S. C.; Dopita, M. A. Abundances of the heavy elements in the Magellanic Clouds. III - Interpretation of results. *ApJ* **1992**, *384*, 508–522.

(6) Westerlund, B. E. *The Magellanic Clouds*; by Bengt E. Westerlund, pp. 292. ISBN 0521480701. Cambridge, UK: Cambridge University Press; 1997.

(7) Dufour, R. J. The composition of H II regions in the Magellanic Clouds. Structure and Evolution of the Magellanic Clouds, Symposium - International Astronomical Union, 108. 1984; pp 353–360.

(8) Koornneef, J. Gas-to-dust ratios in the Magellanic Clouds. Structure and Evolution of the Magellanic Clouds, Symposium - International Astronomical Union, 108. 1984; pp 333–339.

(9) Roman-Duval, J. et al. Dust and Gas in the Magellanic Clouds from the HERITAGE Herschel Key Project. II. Gas-to-dust Ratio Variations across Interstellar Medium Phases. *ApJ* **2014**, *797*, 86.

(10) van Loon, J. T.; Oliveira, J. M.; Gordon, K. D.; Sloan, G. C.; Engelbracht, C. W. A Spitzer Space Telescope Far-infrared Spectral Atlas of Compact Sources in the Magellanic Clouds. II. The Small Magellanic Cloud. *AJ* **2010**, *139*, 1553–1565.

(11) Oliveira, J. M.; van Loon, J. T.; Sloan, G. C.; Indebetouw, R.; Kemper, F.; Tielens, A. G. G. M.; Simon, J. D.; Woods, P. M.; Meixner, M. Ice chemistry in massive young stellar objects: the role of metallicity. *MNRAS* **2011**, *411*, L36–L40.

(12) Browning, M. K.; Tumlinson, J.; Shull, J. M. Inferring Physical Conditions in Interstellar Clouds of H_2. *ApJ* **2003**, *582*, 810–822.

(13) Abdo, A. A. et al. Observations of the Large Magellanic Cloud with Fermi. *A&A* **2010**, *512*, A7.

(14) Knödlseder, J. GeV Gamma-Ray Emission from Normal and Starburst Galaxies. Cosmic Rays in Star-Forming Environments, Astrophysics and Space Science Proceedings, 13. 2013; p 169.

(15) Pei, Y. C.; Fall, S. M.; Hauser, M. G. Cosmic Histories of Stars, Gas, Heavy Elements, and Dust in Galaxies. *ApJ* **1999**, *522*, 604–626.

(16) Heikkilä, A.; Johansson, L. E. B.; Olofsson, H. Molecular abundance variations in the Magellanic Clouds. *A&A* **1999**, *344*, 817–847.

(17) Wang, M.; Chin, Y.-N.; Henkel, C.; Whiteoak, J. B.; Cunningham, M. Abundances and Isotope Ratios in the Magellanic Clouds: The Star-Forming Environment of N 113. *ApJ* **2009**, *690*, 580–597.

(18) Sewiło, M.; Indebetouw, R.; Charnley, S. B.; Zahorecz, S.; Oliveira, J. M.; van Loon, J. T.; Ward, J. L.; Chen, C.-H. R.; Wiseman, J.; Fukui, Y.; Kawamura, A.; Meixner, M.; Onishi, T.; Schilke, P. The Detection of Hot Cores and Complex Organic Molecules in the Large Magellanic Cloud. *ApJ Letters* **2018**, *853*, L19.

(19) Shimonishi, T.; Watanabe, Y.; Nishimura, Y.; Aikawa, Y.; Yamamoto, S.; Onaka, T.; Sakai, N.; Kawamura, A. A Multiline Study of a High-mass Young Stellar Object in the Small Magellanic Cloud with ALMA: The Detection of Methanol Gas at 0.2 Solar Metallicity. *ApJ* **2018**, *862*, 102.

(20) McGuire, B. A. 2018 Census of Interstellar, Circumstellar, Extragalactic, Protoplanetary Disk, and Exoplanetary Molecules. *ApJS* **2018**, *239*, 17.

(21) Meixner, M. et al. The HERSCHEL Inventory of The Agents of Galaxy Evolution in the Magellanic Clouds, a Herschel Open Time Key Program. *AJ* **2013**, *146*, 62.

(22) Cohen, R. S.; Dame, T. M.; Garay, G.; Montani, J.; Rubio, M.; Thaddeus, P. A complete CO survey of the Large Magellanic Cloud. *ApJ Letters* **1988**, *331*, L95–L99.

(23) Rubio, M.; Garay, G.; Montani, J.; Thaddeus, P. A (C-12)O survey of the Small Magellanic Cloud. *ApJ* **1991**, *368*, 173–177.

(24) Fukui, Y. et al. First Results of a CO Survey of the Large Magellanic Cloud with NANTEN; Giant Molecular Clouds as Formation Sites of Populous Clusters. *PASJ* **1999**, *51*, 745–749.

(25) Mizuno, N.; Rubio, M.; Mizuno, A.; Yamaguchi, R.; Onishi, T.; Fukui, Y. First Results of a CO Survey of the Small Magellanic Cloud with NANTEN. *PASJ* **2001**, *53*, L45–L49.

(26) Fukui, Y.; Kawamura, A.; Minamidani, T.; Mizuno, Y.; Kanai, Y.; Mizuno, N.; Onishi, T.; Yonekura, Y.; Mizuno, A.; Ogawa, H.; Rubio, M. The Second Survey of the

Molecular Clouds in the Large Magellanic Cloud by NANTEN. I. Catalog of Molecular Clouds. *ApJS* **2008**, *178*, 56–70.

(27) Wong, T. et al. The Magellanic Mopra Assessment (MAGMA). I. The Molecular Cloud Population of the Large Magellanic Cloud. *ApJS* **2011**, *197*, 16.

(28) Israel, F. P.; Johansson, L. E. B.; Lequeux, J.; Booth, R. S.; Nyman, L. A.; Crane, P.; Rubio, M.; de Graauw, T.; Kutner, M. L.; Gredel, R.; Boulanger, F.; Garay, G.; Westerlund, B. Results of the ESO / SEST Key Programme on Co/ in the Magellanic Clouds - Part One - a Survey of Co/ in the Large Magellanic Cloud and the Small Magellanic Cloud. *A&A* **1993**, *276*, 25.

(29) Israel, F. P.; Johansson, L. E. B.; Rubio, M.; Garay, G.; de Graauw, T.; Booth, R. S.; Boulanger, F.; Kutner, M. L.; Lequeux, J.; Nyman, L.-A. Results of the ESO-SEST Key Programme on CO in the Magellanic Clouds. X. CO emission from star formation regions in LMC and SMC. *A&A* **2003**, *406*, 817–828.

(30) Heikkila, A.; Johansson, L. E. B.; Olofsson, H. The C^18O/C^17O ratio in the Large Magellanic Cloud. *A&A* **1998**, *332*, 493–502.

(31) Johansson, L. E. B.; Olofsson, H.; Hjalmarson, A.; Gredel, R.; Black, J. H. Interstellar molecules in the Large Magellanic Cloud. *A&A* **1994**, *291*, 89–105.

(32) Chin, Y.-N.; Henkel, C.; Whiteoak, J. B.; Millar, T. J.; Hunt, M. R.; Lemme, C. Molecular abundances in the Magellanic Clouds. I. A multiline study of five cloud cores. *A&A* **1997**, *317*, 548–562.

(33) Chin, Y.-N.; Henkel, C.; Millar, T. J.; Whiteoak, J. B.; Marx-Zimmer, M. Molecular abundances in the Magellanic Clouds. III. LIRS36, a star-forming region in the Small Magellanic Cloud. *A&A* **1998**, *330*, 901–909.

(34) Wong, T.; Whiteoak, J. B.; Ott, J.; Chin, Y.-n.; Cunningham, M. R. Synthesis Imaging of Dense Molecular Gas in the N113 H II Region of the Large Magellanic Cloud. *ApJ* **2006**, *649*, 224–234.

(35) Seale, J. P.; Looney, L. W.; Wong, T.; Ott, J.; Klein, U.; Pineda, J. L. The Life and Death of Dense Molecular Clumps in the Large Magellanic Cloud. *ApJ* **2012**, *751*, 42.

(36) Ott, J.; Henkel, C.; Staveley-Smith, L.; Weiß, A. First Detection of Ammonia in the Large Magellanic Cloud: The Kinetic Temperature of Dense Molecular Cores in N 159 W. *ApJ* **2010**, *710*, 105–111.

(37) Nishimura, Y.; Shimonishi, T.; Watanabe, Y.; Sakai, N.; Aikawa, Y.; Kawamura, A.; Yamamoto, S. Spectral Line Survey toward Molecular Clouds in the Large Magellanic Cloud. *ApJ* **2016**, *818*, 161.

(38) Green, J. A. et al. Multibeam maser survey of methanol and excited OH in the Magellanic Clouds: new detections and maser abundance estimates. *MNRAS* **2008**, *385*, 948–956.

(39) Sinclair, M. W.; Carrad, G. J.; Caswell, J. L.; Norris, R. P.; Whiteoak, J. B. A methanol maser in the Large Magellanic Cloud. *MNRAS* **1992**, *256*, 33P.

(40) Ellingsen, S. P.; Whiteoak, J. B.; Norris, R. P.; Caswell, J. L.; Vaile, R. A. A Search for Methanol Masers in the Magellanic Clouds. *MNRAS* **1994**, *269*, 1019.

(41) Beasley, A. J.; Ellingsen, S. P.; Claussen, M. J.; Wilcots, E. A Methanol Maser Survey of IRAS-selected Regions in the Magellanic Clouds. *ApJ* **1996**, *459*, 600.

(42) Ellingsen, S. P.; Breen, S. L.; Caswell, J. L.; Quinn, L. J.; Fuller, G. A. Masers associated with high-mass star formation regions in the Large Magellanic Cloud. *MNRAS* **2010**, *404*, 779–791.

(43) Werner, M. W. et al. The Spitzer Space Telescope Mission. *ApJS* **2004**, *154*, 1–9.

(44) Pilbratt, G. L.; Riedinger, J. R.; Passvogel, T.; Crone, G.; Doyle, D.; Gageur, U.; Heras, A. M.; Jewell, C.; Metcalfe, L.; Ott, S.; Schmidt, M. Herschel Space Observatory. An ESA facility for far-infrared and submillimetre astronomy. *A&A* **2010**, *518*, L1.

(45) Meixner, M. et al. Spitzer Survey of the Large Magellanic Cloud: Surveying the Agents of a Galaxy's Evolution (SAGE). I. Overview and Initial Results. *AJ* **2006**, *132*, 2268–2288.

(46) Gordon, K. D. et al. Surveying the Agents of Galaxy Evolution in the Tidally Stripped, Low Metallicity Small Magellanic Cloud (SAGE-SMC). I. Overview. *AJ* **2011**, *142*, 102.

(47) Whitney, B. A. et al. Spitzer Sage Survey of the Large Magellanic Cloud. III. Star Formation and ˜1000 New Candidate Young Stellar Objects. *AJ* **2008**, *136*, 18–43.

(48) Gruendl, R. A.; Chu, Y. High- and Intermediate-Mass Young Stellar Objects in the Large Magellanic Cloud. *ApJS* **2009**, *184*, 172–197.

(49) Chen, C.-H. R.; Indebetouw, R.; Chu, Y.-H.; Gruendl, R. A.; Testor, G.; Heitsch, F.; Seale, J. P.; Meixner, M.; Sewilo, M. Spitzer View of Young Massive Stars in the Large Magellanic Cloud H II Complexes. II. N 159. *ApJ* **2010**, *721*, 1206–1232.

(50) Romita, K. A.; Carlson, L. R.; Meixner, M.; Sewiło, M.; Whitney, B.; Babler, B.; Indebetouw, R.; Hora, J. L.; Meade, M.; Shiao, B. Young Stellar Objects in the Large Magellanic Cloud Star-forming Region N206. *ApJ* **2010**, *721*, 357–368.

(51) Carlson, L. R.; Sewiło, M.; Meixner, M.; Romita, K. A.; Lawton, B. Identifying young stellar objects in nine Large Magellanic Cloud star-forming regions. *A&A* **2012**, *542*, A66.

(52) Sewiło, M. et al. Surveying the Agents of Galaxy Evolution in the Tidally Stripped, Low Metallicity Small Magellanic Cloud (SAGE-SMC). III. Young Stellar Objects. *ApJ* **2013**, *778*, 15.

(53) Sewiło, M. et al. The youngest massive protostars in the Large Magellanic Cloud. *A&A* **2010**, *518*, L73.

(54) Seale, J. P. et al. Herschel Key Program Heritage: a Far-Infrared Source Catalog for the Magellanic Clouds. *AJ* **2014**, *148*, 124.

(55) Ita, Y. et al. AKARI IRC Survey of the Large Magellanic Cloud: Outline of the Survey and Initial Results. *PASJ* **2008**, *60*, S435–S451.

(56) Kato, D.; Ita, Y.; Onaka, T.; Tanabé, T.; Shimonishi, T.; Sakon, I.; Kaneda, H.; Kawamura, A.; Wada, T.; Usui, F.; Koo, B.-C.; Matsuura, M.; Takahashi, H. AKARI Infrared Camera Survey of the Large Magellanic Cloud. I. Point-source Catalog. *AJ* **2012**, *144*, 179.

(57) Shimonishi, T.; Onaka, T.; Kato, D.; Sakon, I.; Ita, Y.; Kawamura, A.; Kaneda, H. AKARI Infrared Camera Survey of the Large Magellanic Cloud. II. The Near-infrared Spectroscopic Catalog. *AJ* **2013**, *145*, 32.

(58) Oliveira, J. M.; van Loon, J. T.; Chen, C.-H. R.; Tielens, A. G. G. M.; Sloan, G. C.; Woods, P. M.; Kemper, F.; Indebetouw, R.; Gordon, K. D.; Boyer, M. L.; Shiao, B.; Madden, S.; Speck, A. K.; Meixner, M.; Marengo, M. Ice Chemistry in Embedded Young Stellar Objects in the Large Magellanic Cloud. *ApJ* **2009**, *707*, 1269–1295.

(59) Oliveira, J. M.; van Loon, J. T.; Sloan, G. C.; Sewiło, M.; Kraemer, K. E.; Wood, P. R.; Indebetouw, R.; Filipović, M. D.; Crawford, E. J.; Wong, G. F.; Hora, J. L.; Meixner, M.; Robitaille, T. P.; Shiao, B.; Simon, J. D. Early-stage young stellar objects in the Small Magellanic Cloud. *MNRAS* **2013**, *428*, 3001–3033.

(60) Seale, J. P.; Looney, L. W.; Chen, C.-H. R.; Chu, Y.-H.; Gruendl, R. A. The Evolution of Massive Young Stellar Objects in the Large Magellanic Cloud. II. Thermal Processing of Circumstellar Ices. *ApJ* **2011**, *727*, 36.

(61) Shimonishi, T.; Onaka, T.; Kato, D.; Sakon, I.; Ita, Y.; Kawamura, A.; Kaneda, H. AKARI Near-Infrared Spectroscopy: Detection of H_2O and CO_2 Ices toward Young Stellar Objects in the Large Magellanic Cloud. *ApJ Letters* **2008**, *686*, L99.

(62) Shimonishi, T.; Onaka, T.; Kato, D.; Sakon, I.; Ita, Y.; Kawamura, A.; Kaneda, H. Spectroscopic observations of ices around embedded young stellar objects in the Large Magellanic Cloud with AKARI. *A&A* **2010**, *514*, A12.

(63) van Dishoeck, E. F. Astrochemistry of dust, ice and gas: introduction and overview. *Faraday Discussions* **2014**, *168*, 9.

(64) Whittet, D. C. B.; Bode, M. F.; Longmore, A. J.; Adamson, A. J.; McFadzean, A. D.; Aitken, D. K.; Roche, P. F. Infrared spectroscopy of dust in the Taurus dark clouds - Ice and silicates. *MNRAS* **1988**, *233*, 321–336.

(65) Pontoppidan, K. M.; Salyk, C.; Bergin, E. A.; Brittain, S.; Marty, B.; Mousis, O.; Öberg, K. I. Volatiles in Protoplanetary Disks. *Protostars and Planets VI* **2014**, 363–385.

(66) Shimonishi, T.; Dartois, E.; Onaka, T.; Boulanger, F. VLT/ISAAC infrared spectroscopy of embedded high-mass YSOs in the Large Magellanic Cloud: Methanol and the 3.47 μm band. *A&A* **2016**, *585*, A107.

(67) Bernard-Salas, J.; Peeters, E.; Sloan, G. C.; Cami, J.; Guiles, S.; Houck, J. R. The Spitzer IRS spectrum of SMP LMC 11. *ApJ Letters* **2006**, *652*, L29–L32.

(68) Tielens, A. G. G. M. Interstellar polycyclic aromatic hydrocarbon molecules. *ARA&A* **2008**, *46*, 289–337.

(69) Malek, S. E.; Cami, J.; Bernard-Salas, J. The Rich Circumstellar Chemistry of SMP LMC 11. *ApJ* **2012**, *744*, 16.

(70) Cernicharo, J.; Heras, A. M.; Tielens, A. G. G. M.; Pardo, J. R.; Herpin, F.; Guélin, M.; Waters, L. B. F. M. Infrared Space Observatory's Discovery of C_4H_2, C_6H_2, and Benzene in CRL 618. *ApJ Letters* **2001**, *546*, L123–L126.

(71) Jones, O. C. et al. The SAGE-Spec Spitzer Legacy program: the life-cycle of dust and gas in the Large Magellanic Cloud. Point source classification - III. *MNRAS* **2017**, *470*, 3250–3282.

(72) Seale, J. P.; Looney, L. W.; Chu, Y.-H.; Gruendl, R. A.; Brandl, B.; Chen, C.-H. R.; Brandner, W.; Blake, G. A. The Evolution Of Massive Young Stellar Objects in the Large Magellanic Cloud. I. Identification and Spectral Classification. *ApJ* **2009**, *699*, 150–167.

(73) Shimonishi, T.; Onaka, T.; Kawamura, A.; Aikawa, Y. The Detection of a Hot Molecular Core in the Large Magellanic Cloud with ALMA. *ApJ* **2016**, *827*, 72.

(74) Kato, D. et al. The IRSF Magellanic Clouds Point Source Catalog. *PASJ* **2007**, *59*, 615–641.

(75) Smith, R. C.; MCELS Team, The UM/CTIO Magellanic Cloud emission-line survey. *PASA* **1998**, *15*, 163–64.

(76) Tokuda, K. et al. An ALMA view of molecular filaments in the Large Magellanic Cloud II: An early stage of high-mass star formation embedded at colliding clouds in N159W-South. *arXiv e-prints* **2018**, *arXiv:1811.04400*.

(77) Fukui, Y. et al. High-mass Star Formation Triggered by Collision between CO Filaments in N159 West in the Large Magellanic Cloud. *ApJ Letters* **2015**, *807*, L4.

(78) Testor, G.; Lemaire, J. L.; Field, D.; Diana, S. VLT/NACO near-infrared imaging and spectroscopy of N159A in the LMC HII complex N159. *A&A* **2006**, *453*, 517–524.

(79) van Loon, J. T.; Cohen, M.; Oliveira, J. M.; Matsuura, M.; McDonald, I.; Sloan, G. C.; Wood, P. R.; Zijlstra, A. A. Molecules and dust production in the Magellanic Clouds. *A&A* **2008**, *487*, 1055–1073.

(80) Ward, J. L.; Oliveira, J. M.; van Loon, J. T.; Sewiło, M. K- band integral field spectroscopy and optical spectroscopy of massive young stellar objects in the Small Magellanic Cloud. *MNRAS* **2017**, *464*, 1512–1552.

(81) Shull, J. M.; Hollenbach, D. J. H2 cooling, dissociation, and infrared emission in shocked molecular clouds. *ApJ* **1978**, *220*, 525–537.

(82) Tielens, A. G. G. M. *The Physics and Chemistry of the Interstellar Medium, by A. G. G. M. Tielens, pp. . ISBN 0521826349. Cambridge, UK: Cambridge University Press, 2005.*; 2005.

(83) Sakai, T.; Sakai, N.; Hirota, T.; Yamamoto, S. A Survey of Molecular Lines Toward Massive Clumps in Early Evolutionary Stages of High-mass Star Formation. *ApJ* **2010**, *714*, 1658–1671.

(84) Oliveira, J. M.; van Loon, J. T.; Stanimirović, S.; Zijlstra, A. A. Massive young stellar objects in the Large Magellanic Cloud: water masers and ESO-VLT 3-4 μm spectroscopy. *MNRAS* **2006**, *372*, 1509–1524.

(85) Whiteoak, J. B.; Gardner, F. F. Observations of H2O masers in nearby galaxies. *MNRAS* **1986**, *222*, 513–523.

(86) Lazendic, J. S.; Whiteoak, J. B.; Klamer, I.; Harbison, P. D.; Kuiper, T. B. H. Accurate positions of H_2 O masers in the Large Magellanic Cloud. *MNRAS* **2002**, *331*, 969–974.

(87) Ward, J. L.; Oliveira, J. M.; van Loon, J. T.; Sewiło, M. Integral field spectroscopy of massive young stellar objects in the N113 H II region in the Large Magellanic Cloud. *MNRAS* **2016**, *455*, 2345–2362.

(88) Fontani, F.; Palau, A.; Caselli, P.; Sánchez-Monge, Á.; Butler, M. J.; Tan, J. C.; Jiménez-Serra, I.; Busquet, G.; Leurini, S.; Audard, M. Deuteration as an evolutionary tracer in massive-star formation. *A&A* **2011**, *529*, L7.

(89) Caselli, P.; Ceccarelli, C. Our astrochemical heritage. *A&AR* **2012**, *20*, 56.

(90) Albertsson, T.; Semenov, D. A.; Vasyunin, A. I.; Henning, T.; Herbst, E. New Extended Deuterium Fractionation Model: Assessment at Dense ISM Conditions and Sensitivity Analysis. *ApJS* **2013**, *207*, 27.

(91) Gerner, T.; Shirley, Y. L.; Beuther, H.; Semenov, D.; Linz, H.; Albertsson, T.; Henning, T. Chemical evolution in the early phases of massive star formation. II. Deuteration. *A&A* **2015**, *579*, A80.

(92) Mookerjea, B.; Casper, E.; Mundy, L. G.; Looney, L. W. Kinematics and Chemistry of the Hot Molecular Core in G34.26+0.15 at High Resolution. *ApJ* **2007**, *659*, 447–458.

(93) Bisschop, S. E.; Jørgensen, J. K.; van Dishoeck, E. F.; de Wachter, E. B. M. Testing grain-surface chemistry in massive hot-core regions. *A&A* **2007**, *465*, 913–929.

(94) Kurtz, S.; Cesaroni, R.; Churchwell, E.; Hofner, P.; Walmsley, C. M. Hot Molecular Cores and the Earliest Phases of High-Mass Star Formation. *Protostars and Planets IV* **2000**, 299–326.

(95) Herbst, E.; van Dishoeck, E. F. Complex Organic Interstellar Molecules. *ARA&A* **2009**, *47*, 427–480.

(96) Widicus Weaver, S. L.; Laas, J. C.; Zou, L.; Kroll, J. A.; Rad, M. L.; Hays, B. M.; Sanders, J. L.; Lis, D. C.; Cross, T. N.; Wehres, N.; McGuire, B. A.; Sumner, M. C.

Deep, Broadband Spectral Line Surveys of Molecule-rich Interstellar Clouds. *ApJS* **2017**, *232*, 3.

(97) Bacmann, A.; Taquet, V.; Faure, A.; Kahane, C.; Ceccarelli, C. Detection of complex organic molecules in a prestellar core: a new challenge for astrochemical models. *A&A* **2012**, *541*, L12.

(98) Cernicharo, J.; Marcelino, N.; Roueff, E.; Gerin, M.; Jiménez-Escobar, A.; Muñoz Caro, G. M. Discovery of the Methoxy Radical, CH_3O, toward B1: Dust Grain and Gas-phase Chemistry in Cold Dark Clouds. *ApJ Letters* **2012**, *759*, L43.

(99) Vastel, C.; Ceccarelli, C.; Lefloch, B.; Bachiller, R. The Origin of Complex Organic Molecules in Prestellar Cores. *ApJ Letters* **2014**, *795*, L2.

(100) Jiménez-Serra, I.; Vasyunin, A. I.; Caselli, P.; Marcelino, N.; Billot, N.; Viti, S.; Testi, L.; Vastel, C.; Lefloch, B.; Bachiller, R. The Spatial Distribution of Complex Organic Molecules in the L1544 Pre-stellar Core. *ApJ Letters* **2016**, *830*, L6.

(101) Taquet, V.; Wirström, E. S.; Charnley, S. B.; Faure, A.; López-Sepulcre, A.; Persson, C. M. Chemical complexity induced by efficient ice evaporation in the Barnard 5 molecular cloud. *A&A* **2017**, *607*, A20.

(102) Minissale, M.; Moudens, A.; Baouche, S.; Chaabouni, H.; Dulieu, F. Hydrogenation of CO-bearing species on grains: unexpected chemical desorption of CO. *MNRAS* **2016**, *458*, 2953–2961.

(103) Chuang, K. J.; Fedoseev, G.; Qasim, D.; Ioppolo, S.; van Dishoeck, E. F.; Linnartz, H. Reactive Desorption of CO Hydrogenation Products under Cold Pre-stellar Core Conditions. *ApJ* **2018**, *853*, 102.

(104) Brown, P. D.; Charnley, S. B.; Millar, T. J. A model of the chemistry in hot molecular cores. *MNRAS* **1988**, *231*, 409–417.

(105) Bergin, E. A.; Tafalla, M. Cold Dark Clouds: The Initial Conditions for Star Formation. *ARA&A* **2007**, *45*, 339–396.

(106) Garrod, R. T.; Herbst, E. Formation of methyl formate and other organic species in the warm-up phase of hot molecular cores. *A&A* **2006**, *457*, 927–936.

(107) Charnley, S. B.; Tielens, A. G. G. M.; Millar, T. J. On the molecular complexity of the hot cores in Orion A - Grain surface chemistry as 'The last refuge of the scoundrel'. *ApJ Letters* **1992**, *399*, L71–L74.

(108) Rodgers, S. D.; Charnley, S. B. Chemical Evolution in Protostellar Envelopes: Cocoon Chemistry. *ApJ* **2003**, *585*, 355–371.

(109) Aikawa, Y.; Wakelam, V.; Garrod, R. T.; Herbst, E. Molecular Evolution and Star Formation: From Prestellar Cores to Protostellar Cores. *ApJ* **2008**, *674*, 984–996.

(110) Gratier, P.; Majumdar, L.; Ohishi, M.; Roueff, E.; Loison, J. C.; Hickson, K. M.; Wakelam, V. A New Reference Chemical Composition for TMC-1. *ApJS* **2016**, *225*, 25.

(111) Maffucci, D. M.; Wenger, T. V.; Le Gal, R.; Herbst, E. Astrochemical Kinetic Grid Models of Groups of Observed Molecular Abundances: Taurus Molecular Cloud 1 (TMC-1). *ApJ* **2018**, *868*, 41.

(112) Sakai, N.; Yamamoto, S. Warm Carbon-Chain Chemistry. *Chem. Rev.* **2013**, *113*, 8981–9015.

(113) Tielens, A. G. G. M.; Hagen, W. Model calculations of the molecular composition of interstellar grain mantles. *A&A* **1982**, *114*, 245–260.

(114) Charnley, S. B.; Rodgers, S. D. Interstellar Reservoirs of Cometary Matter. *Space Science Reviews* **2008**, *138*, 59–73.

(115) Charnley, S. Interstellar Organic Chemistry. The Bridge Between the Big Bang and Biology: Stars, Planetary Systems, Atmospheres, Volcanoes: Their Link to Life, International workshop, Stromboli, Italy, September 13-17, 1999 Rome: Consiglio Nazionale delle Ricerche, Edited by Franco Giovanelli. 2001; p 139.

(116) Hollis, J. M.; Lovas, F. J.; Jewell, P. R. Interstellar Glycolaldehyde: The First Sugar. *ApJ Letters* **2000**, *540*, L107–L110.

(117) Hollis, J. M.; Jewell, P. R.; Lovas, F. J.; Remijan, A. Green Bank Telescope Observations of Interstellar Glycolaldehyde: Low-Temperature Sugar. *ApJ Letters* **2004**, *613*, L45–L48.

(118) Hollis, J. M.; Lovas, F. J.; Jewell, P. R.; Coudert, L. H. Interstellar Antifreeze: Ethylene Glycol. *ApJ Letters* **2002**, *571*, L59–L62.

(119) Hollis, J. M.; Jewell, P. R.; Lovas, F. J.; Remijan, A.; Møllendal, H. Green Bank Telescope Detection of New Interstellar Aldehydes: Propenal and Propanal. *ApJ Letters* **2004**, *610*, L21–L24.

(120) Watanabe, N.; Kouchi, A. Ice surface reactions: A key to chemical evolution in space. *Progress in Surface Science* **2008**, *83*, 439–489.

(121) Ioppolo, S.; Cuppen, H. M.; Linnartz, H. Surface formation routes of interstellar molecules: hydrogenation reactions in simple ices. *Rend. Fis. Acc. Lincei* **2011**, *22*, 211.

(122) Linnartz, H.; Ioppolo, S.; Fedoseev, G. Atom addition reactions in interstellar ice analogues. *International Reviews in Physical Chemistry* **2015**, *34*, 205–237.

(123) Caselli, P.; Hasegawa, T. I.; Herbst, E. Chemical differentiation between star-forming regions - The Orion Hot Core and Compact Ridge. *ApJ* **1993**, *408*, 548–558.

(124) Rodgers, S. D.; Charnley, S. B. Chemical Differentiation in Regions of Massive Star Formation. *ApJ* **2001**, *546*, 324–329.

(125) Blake, G. A.; Sutton, E. C.; Masson, C. R.; Phillips, T. G. Molecular abundances in OMC-1 - The chemical composition of interstellar molecular clouds and the influence of massive star formation. *ApJ* **1987**, *315*, 621–645.

(126) Charnley, S. B.; Kress, M. E.; Tielens, A. G. G. M.; Millar, T. J. Interstellar Alcohols. *ApJ* **1995**, *448*, 232.

(127) Karpas, Z.; Mautner, M. Alkyl-transfer reactions between protonated alcohols and ethers: gas-phase alkylation of formaldehyde. *J. Phys. Chem.* **1989**, *93*, 1859–63.

(128) Cole, C. A.; Wehres, N.; Yang, Z.; Thomsen, D. L.; Snow, T. P.; Bierbaum, V. M. A Gas-phase Formation Route to Interstellar Trans-methyl Formate. *ApJ Letters* **2012**, *754*, L5.

(129) Neill, J. L.; Steber, A. L.; Muckle, M. T.; Zaleski, D. P.; Lattanzi, V.; Spezzano, S.; McCarthy, M. C.; Remijan, A. J.; Friedel, D. N.; Widicus Weaver, S. L.; Pate, B. H. Spatial Distributions and Interstellar Reaction Processes. *J. Phys. Chem.* **2011**, *115*, 6472–6480.

(130) Neill, J. L.; Muckle, M. T.; Zaleski, D. P.; Steber, A. L.; Pate, B. H.; Lattanzi, V.; Spezzano, S.; McCarthy, M. C.; Remijan, A. J. Laboratory and Tentative Interstellar Detection of Trans-Methyl Formate Using the Publicly Available Green Bank Telescope Primos Survey. *ApJ* **2012**, *755*, 153.

(131) Taquet, V.; Wirström, E. S.; Charnley, S. B. Formation and Recondensation of Complex Organic Molecules during Protostellar Luminosity Outbursts. *ApJ* **2016**, *821*, 46.

(132) Laas, J. C.; Garrod, R. T.; Herbst, E.; Widicus Weaver, S. L. Contributions from Grain Surface and Gas Phase Chemistry to the Formation of Methyl Formate and Its Structural Isomers. *ApJ* **2011**, *728*, 71.

(133) Belloche, A.; Garrod, R. T.; Müller, H. S. P.; Menten, K. M.; Comito, C.; Schilke, P. Increased complexity in interstellar chemistry: detection and chemical modeling of ethyl formate and n-propyl cyanide in Sagittarius B2(N). *A&A* **2009**, *499*, 215–232.

(134) Tercero, B.; Cernicharo, J.; López, A.; Brouillet, N.; Kolesniková, L.; Motiyenko, R. A.; Margulès, L.; Alonso, J. L.; Guillemin, J.-C. Searching for trans ethyl methyl ether in Orion KL. *A&A* **2015**, *582*, L1.

(135) Hamberg, M.; Österdahl, F.; Thomas, R. D.; Zhaunerchyk, V.; Vigren, E.; Kaminska, M.; Af Ugglas, M.; Källberg, A.; Simonsson, A.; Paál, A.; Larsson, M.; Geppert, W. D. Experimental studies of the dissociative recombination processes for the dimethyl ether ions $CD_3OCD_2^+$ and $(CD_3)_2OD^+$. *A&A* **2010**, *514*, A83.

(136) Boogert, A. C. A.; Gerakines, P. A.; Whittet, D. C. B. Observations of the icy universe. *ARA&A* **2015**, *53*, 541–581.

(137) Skouteris, D.; Balucani, N.; Ceccarelli, C.; Faginas Lago, N.; Codella, C.; Falcinelli, S.; Rosi, M. Interstellar dimethyl ether gas-phase formation: a quantum chemistry and kinetics study. *MNRAS* **2019**, *482*, 3567–3575.

(138) Cernicharo, J.; Kisiel, Z.; Tercero, B.; Kolesniková, L.; Medvedev, I. R.; López, A.; Fortman, S.; Winnewisser, M.; de Lucia, F. C.; Alonso, J. L.; Guillemin, J. C. A rigorous detection of interstellar CH_3NCO: An important missing species in astrochemical networks. *A&A* **2016**, *587*, L4.

(139) Hollis, J. M.; Lovas, F. J.; Remijan, A. J.; Jewell, P. R.; Ilyushin, V. V.; Kleiner, I. Detection of Acetamide (CH_3CONH_2): The Largest Interstellar Molecule with a Peptide Bond. *ApJ Letters* **2006**, *643*, L25–L28.

(140) Shingledecker, C. N.; Tennis, J.; Le Gal, R.; Herbst, E. On Cosmic-Ray-driven Grain Chemistry in Cold Core Models. *ApJ* **2018**, *861*, 20.

(141) Benz, A. O. et al. Hydrides in young stellar objects: Radiation tracers in a protostar-disk-outflow system. *A&A* **2010**, *521*, L35.

(142) Prasad, S. S.; Tarafdar, S. P. UV radiation field inside dense clouds - Its possible existence and chemical implications. *ApJ* **1983**, *267*, 603–609.

(143) Bernstein, M. P.; Sandford, S. A.; Allamandola, L. J.; Chang, S.; Scharberg, M. A. Organic Compounds Produced by Photolysis of Realistic Interstellar and Cometary Ice Analogs Containing Methanol. *ApJ* **1995**, *454*, 327.

(144) Öberg, K. I.; Garrod, R. T.; van Dishoeck, E. F.; Linnartz, H. Formation rates of complex organics in UV irradiated CH_3OH-rich ices. I. Experiments. *A&A* **2009**, *504*, 891–913.

(145) Allen, M.; Robinson, G. W. The molecular composition of dense interstellar clouds. *ApJ* **1977**, *212*, 396–415.

(146) D'Hendecourt, L. B.; Allamandola, L. J.; Grim, R. J. A.; Greenberg, J. M. Time-dependent chemistry in dense molecular clouds. II - Ultraviolet photoprocessing and infrared spectroscopy of grain mantles. *A&A* **1986**, *158*, 119–134.

(147) Brown, P. D. The grain-surface formation of complex molecules. *MNRAS* **1990**, *243*, 65–71.

(148) Hollis, J. M.; Vogel, S. N.; Snyder, L. E.; Jewell, P. R.; Lovas, F. J. The Spatial Scale of Glycolaldehyde in the Galactic Center. *ApJ Letters* **2001**, *554*, L81–L85.

(149) Sorrell, W. H. Origin of Amino Acids and Organic Sugars in Interstellar Clouds. *ApJ Letters* **2001**, *555*, L129–L132.

(150) Viti, S.; Williams, D. A. Time-dependent evaporation of icy mantles in hot cores. *MNRAS* **1999**, *305*, 755–762.

(151) Garrod, R. T.; Widicus Weaver, S. L.; Herbst, E. Complex Chemistry in Star-forming Regions: An Expanded Gas-Grain Warm-up Chemical Model. *ApJ* **2008**, *682*, 283–302.

(152) Ligterink, N. F. W.; Coutens, A.; Kofman, V.; Müller, H. S. P.; Garrod, R. T.; Calcutt, H.; Wampfler, S. F.; Jørgensen, J. K.; Linnartz, H.; van Dishoeck, E. F. The ALMA-PILS survey: detection of CH_3NCO towards the low-mass protostar IRAS 16293-2422 and laboratory constraints on its formation. *MNRAS* **2017**, *469*, 2219–2229.

(153) Millar, T. J.; Herbst, E. Chemical modelling of dark clouds in the LMC and SMC. *MNRAS* **1990**, *242*, 92–97.

(154) Acharyya, K.; Herbst, E. Molecular Development in the Large Magellanic Cloud. *ApJ* **2015**, *812*, 142.

(155) Acharyya, K.; Herbst, E. Simulations of the Chemistry in the Small Magellanic Cloud. *ApJ* **2016**, *822*, 105.

(156) Collings, M. P.; Anderson, M. A.; Chen, R.; Dever, J. W.; Viti, S.; Williams, D. A.; McCoustra, M. R. S. A laboratory survey of the thermal desorption of astrophysically relevant molecules. *MNRAS* **2004**, *354*, 1133–1140.

(157) Pauly, T.; Garrod, R. T. Modeling CO, CO_2, and H_2O Ice Abundances in the Envelopes of Young Stellar Objects in the Magellanic Clouds. *ApJ* **2018**, *854*, 13.

(158) Acharyya, K.; Herbst, E. Hot Cores in Magellanic Clouds. *ApJ* **2018**, *859*, 51.

(159) Audard, M.; Ábrahám, P.; Dunham, M. M.; Green, J. D.; Grosso, N.; Hamaguchi, K.; Kastner, J. H.; Kóspál, Á.; Lodato, G.; Romanova, M. M.; Skinner, S. L.;

Vorobyov, E. I.; Zhu, Z. Episodic Accretion in Young Stars. *Protostars and Planets VI* **2014**, 387–410.

(160) Buckle, J. V.; Rodgers, S. D.; Wirstrom, E. S.; Charnley, S. B.; Markwick-Kemper, A. J.; Butner, H. M.; Takakuwa, S. Observations of chemical differentiation in clumpy molecular clouds. *Faraday Discussions* **2006**, *133*, 63–82.

(161) Wirström, E. S.; Charnley, S. B.; Persson, C. M.; Buckle, J. V.; Cordiner, M. A.; Takakuwa, S. Cold Water Vapor in the Barnard 5 Molecular Cloud. *ApJ Letters* **2014**, *788*, L32.

(162) Mumma, M. J.; Charnley, S. B. The Chemical Composition of Comets - Emerging Taxonomies and Natal Heritage. *ARA&A* **2011**, *49*, 471–524.

(163) Oliveira, J. M. The star formation process in the Magellanic Clouds. The Magellanic System: Stars, Gas, and Galaxies, Symposium - International Astronomical Union, 256, Edited by J. T. van Loon and J. M. Oliveira. 2009; pp 191–202.

(164) Fedoseev, G.; Chuang, K.-J.; Ioppolo, S.; Qasim, D.; van Dishoeck, E. F.; Linnartz, H. Formation of Glycerol through Hydrogenation of CO Ice under Prestellar Core Conditions. *ApJ* **2017**, *842*, 52.

Graphical TOC Entry

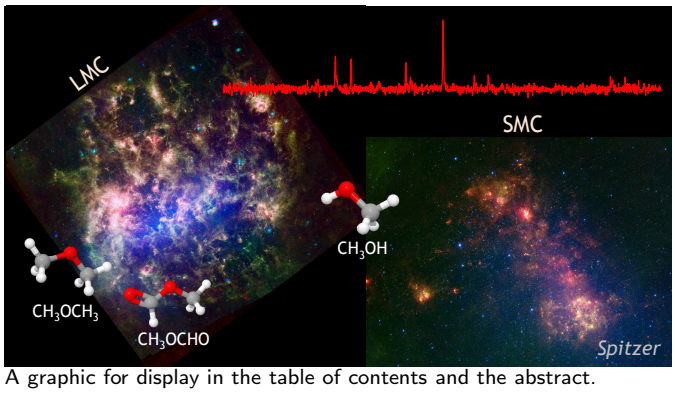

A graphic for display in the table of contents and the abstract.